We now report the establishment of infectious virion-producing replicon cells that utilize an ordinary genotype 1b replicon strain. In order to address the contribution of structural and non-structural gene products to the maturation of HCV particles in vitro, we partitioned these regions in the same cistron of the full genomic sequence, thereby enabling the functions of these structural and non-structural genes to be studied separately. Thus, we termed this construction "divided open reading frame carrying" full genome replicon, or dORF replicon.

Virus particles secreted from cells containing dORF replicon RNA, as confirmed morphologically using electron microscopy, were shown to be able to infect Huh-7 cells. Replication of dORF replicon RNA was so efficient that infected cells could survive and proliferate under G418 selection to form colonies, as seen after transfection with replicon RNA. In addition, a reporter gene was successfully inserted into the construct, and activity of the reporter gene could be transmitted to naive Huh-7 cells by infection.

We believe that the success of this system is due to the difference in the construction of the replicon, namely, having the intact 5′ half extending to NS2 instead of being divided at the beginning of the core region. Although further investigation is required to elucidate whether the encapsidation signal of HCV is located in the region that is divided in the full-genome replicon, this is the first report to describe genome-length replicon-containing cells that can produce virus particles that have the putative characteristics of the HCV virion, in terms of both morphology and biological properties.

Results

dORF replicon RNA can replicate in Huh-7 cells

We began this study with transfection with the dORF replicon RNAs (Fig. 1A). When 30 μg of each RNA was electroporated into 4×10^6 Huh-7 cells, the dORF and dORF bla RNA-transfected cells formed 20 and 5 colonies, respectively, after 3 weeks of G418 selection. No colonies appeared as a result of transfection with polymerase-defective mutants (data not shown). Two colonies were picked, amplified, and designated as dORF replicon cell #1 and #2, and dORF bla replicon cell #1 and #2. Some of these cells were then used for quantification of HCV RNA and northern blot analysis (Fig. 1B). Northern blot analysis showed that these clones contained HCV RNAs of the expected size and that the HCV RNA copy numbers of these clones did not differ substantially from that of the subgenomic replicon, indicating that replication ability had not been hampered by insertion of the structural genes, which is counter to what was expected. Western blot analysis showed that these clones express both structural and non-structural proteins (Fig. 1C). These results confirmed that transfected dORF HCV RNAs can replicate in Huh-7 cells, just as authentic subgenomic replicon RNAs do.

dORF replicon cells secrete virus particles

In a previous study, HCV subgenomic replicon cells secreted RNase-resistant subgenomic RNA into the culture supernatant [4, 7, 20]. We also detected a similar amount of RNase-resistant HCV RNA in the culture supernatant of our dORF replicon cells, as well as of the subgenomic and full-genome replicon cells. These supernatants showed no significant differences in terms of distribution of HCV RNA in buoyant density gradient analysis (Figs. 2A, B, open square). In contrast, there was a clear difference between these supernatants after NP-40 treatment. While almost all of the HCV RNA in the supernatant of the subgenomic replicon cells was eliminated by NP-40 treatment (Fig. 2A, filled triangle), there remained a peak of HCV RNA at a density of 1.18 g/mL in the supernatant of the dORF replicon cells (Fig. 2B, filled triangle). These results were confirmed in the same experiment, using concentrated culture supernatant (Figs. 2C, D). We also confirmed the results of previous reports [7, 20], which showed no genomic RNA resistant to NP-40 treatment in the supernatant of full-genome replicon cells (Fig. 2E). Secreted core proteins in the concentrated supernatant showed a different density gradient distribution compared to genomic RNA (Fig. 2F, open circle) in that the core proteins were present at densities of 1.1–1.2 g/mL, while HCV RNA was more broadly distributed in the range of 1.06–1.22 g/mL. Thus, HCV RNA and core proteins were not always associated with each other. However, after NP-40 treatment, core proteins were found only in the same fraction as HCV RNA, at 1.19 g/mL (Fig. 2F, filled triangle). Taken together with the results of the report mentioned above [20], our replicon cells harboring dORF RNA appeared to secrete particles with core proteins that were assembled into nucleocapsids as well as particles without core proteins that were sensitive to NP-40 treatment, like the ones from subgenomic and full-genome replicon cells. We concluded that the broader distribution of the HCV genome RNA in the density gradient than that of the core protein was caused by the overlapping distribution of these two particle types, and that the remaining peaks of genome RNA and core protein after NP-40 treatment were of nucleocapsids that had had their envelopes stripped off by NP-40 [11].

According to our hypothesis, the distribution of core proteins in the density gradient represented that of the

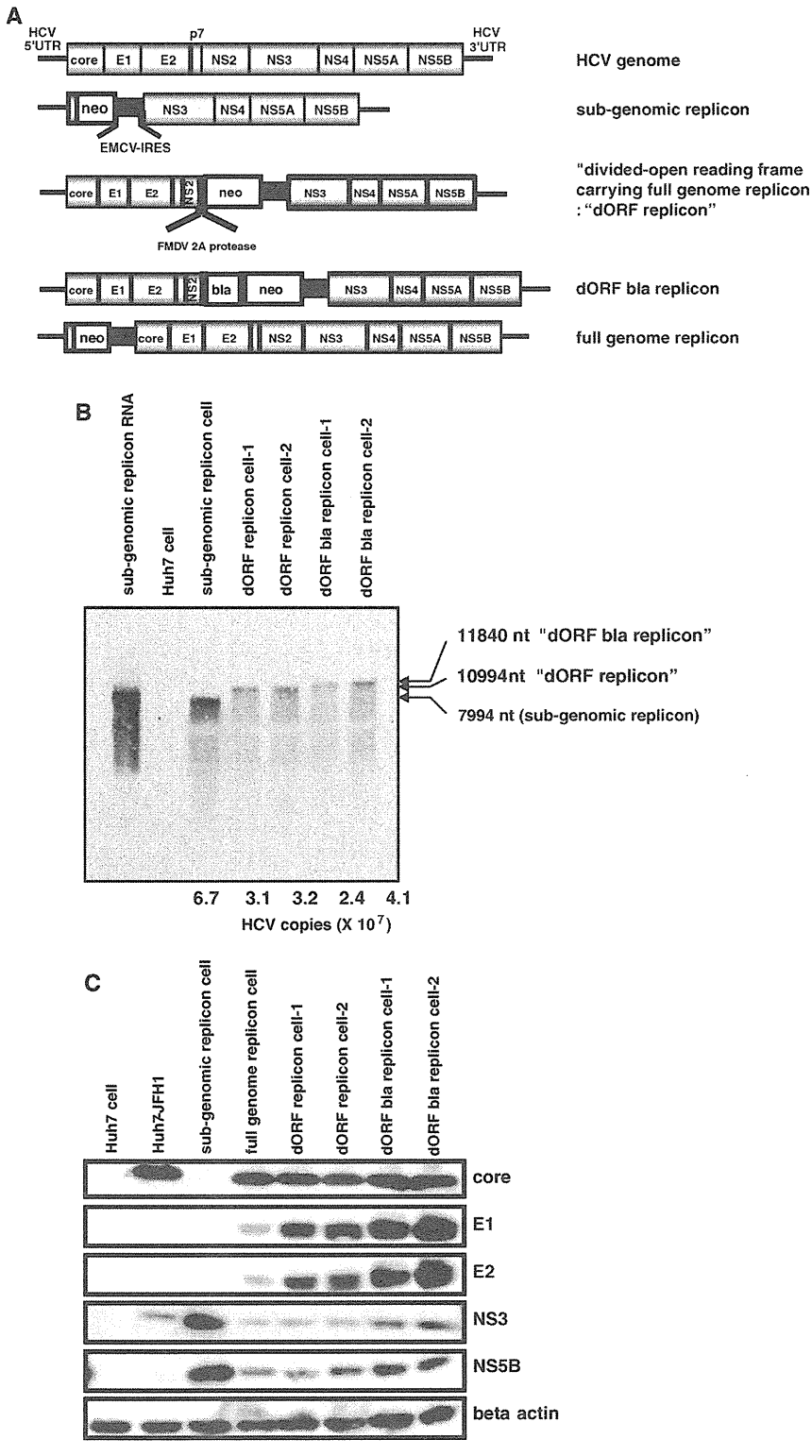

Fig. 1 Confirmation of "divided open reading frame carrying" (dORF) replicon cells. (A) Schematic representations of replicon RNAs used in this study. All the replicon constructs contained inserts just after the T7 promotor. UTR, untranslated region; NS, non-structural protein; neo, neomycin phosphotransferase II; EMCV, encephalomyocarditis virus; IRES, internal ribosomal entry site; FMDV, foot-and-mouth disease virus; bla, beta-lactamase. (B) Northern blot analysis. A 10-μg amount of total RNA from each cell sample was loaded. Subgenomic replicon RNA: 10^8 copies of in vitro-generated subgenomic RNA. Numbers below the lanes are the HCV copy number per microgram of total RNA. Huh-7 cell, subgenomic replicon cell, dORF replicon cell #1, #2, dORF bla replicon cell #1, #2. (C) Western blot analysis. A 10-μg amount of each cell lysate was loaded. Huh-7 cell, Huh-7-JFH1: Huh-7 cell transfected with JFH1 viral RNA, subgenomic replicon cell, full-genome replicon cell, dORF replicon cell #1, #2, dORF bla replicon cell #1, #2

intact virion, and we therefore tried to observe virions directly by electron microscopy, using the fraction in which the core protein was present. We easily identified numerous round-shaped virus particles approximately 50 nm in diameter by scanning electron microscopy (Fig. 3A). Furthermore, when the immunogold method using anti-E2

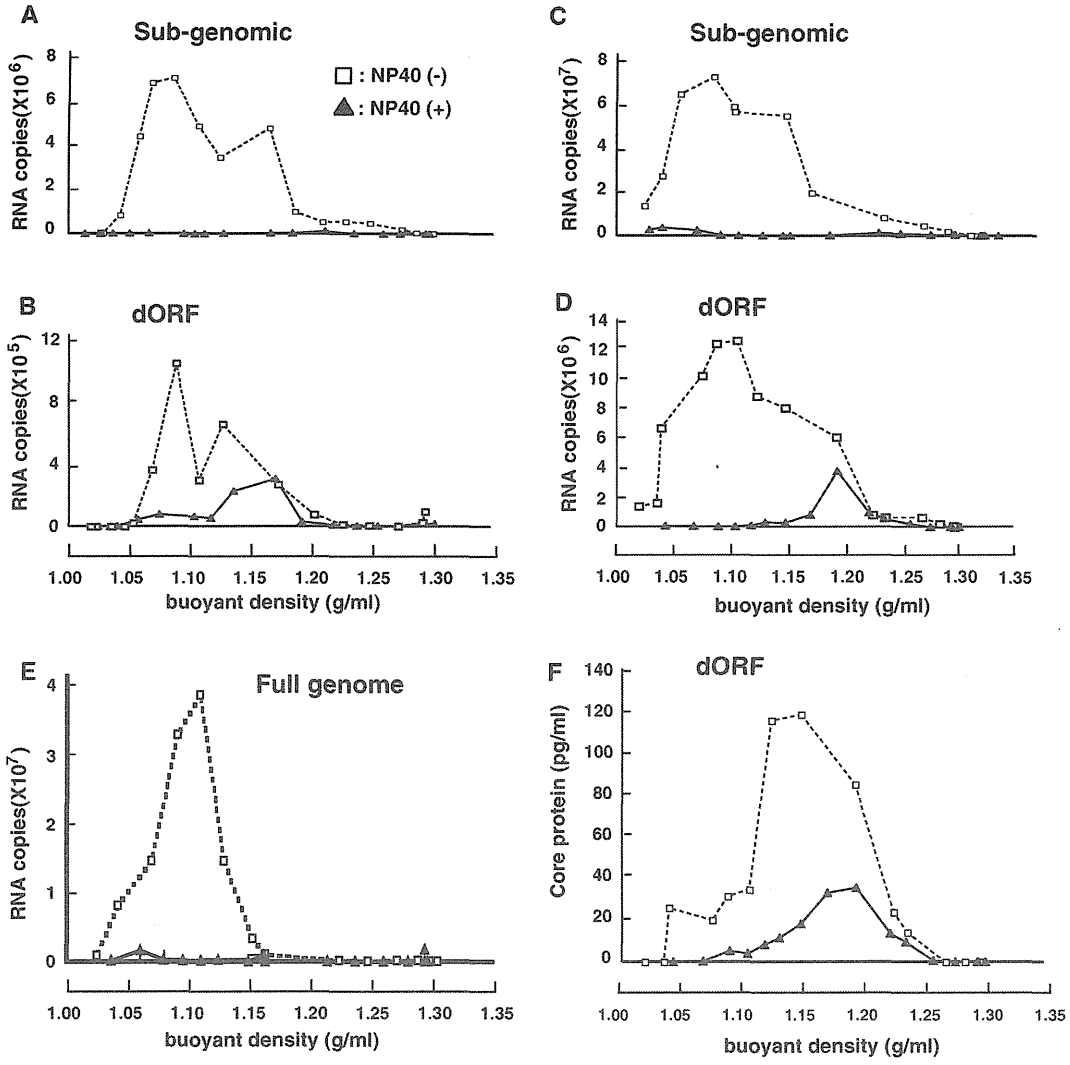

Fig. 2 Density gradient analysis of supernatants. Culture supernatants were treated with RNaseA and loaded directly onto a sucrose density gradient without treatment (open square) or after NP-40 treatment (filled triangle). Quantification of HCV RNA in each fraction of supernatant from the subgenomic replicon (A) and dORF replicon (B). Analysis of concentrated culture supernatant from the subgenomic replicon (C) and dORF replicon (D). Concentrated culture supernatant from the full-genome replicon NNC#2 was also analyzed (E). Quantification of HCV core protein in each fraction of supernatant from the dORF replicon (F)

RR6 antibody was applied to samples fixed on the mesh, transmission electron microscopy could be used to visualize virus particles labeled with colloidal gold (Fig. 3B). These findings provide evidence of intact virion production from our dORF replicon cells.

Secreted virus particles can infect naive Huh-7 cells

Next, we examined the infectivity of these virus particles. The culture supernatants of these dORF replicon cells were collected, and 3 kinds of naive Huh-7 cells, one purchased from the J.C.R.B. (Japanese Collection of Research Bioresources) and the other two, designated as the cured cells F2 and K4, generated by IFN-α treatment of 1bneo/delS replicon cells, were infected with these supernatants. After two sequential passages and three weeks of G418 selection as described above, a number of colonies appeared, as shown in Fig. 4A. The largest number of colonies was produced from the cured cells K4, and slightly fewer colonies were produced from the cured cells F2, while no colonies appeared when normal Huh-7 cells were used (data not shown). The same infection experiment carried

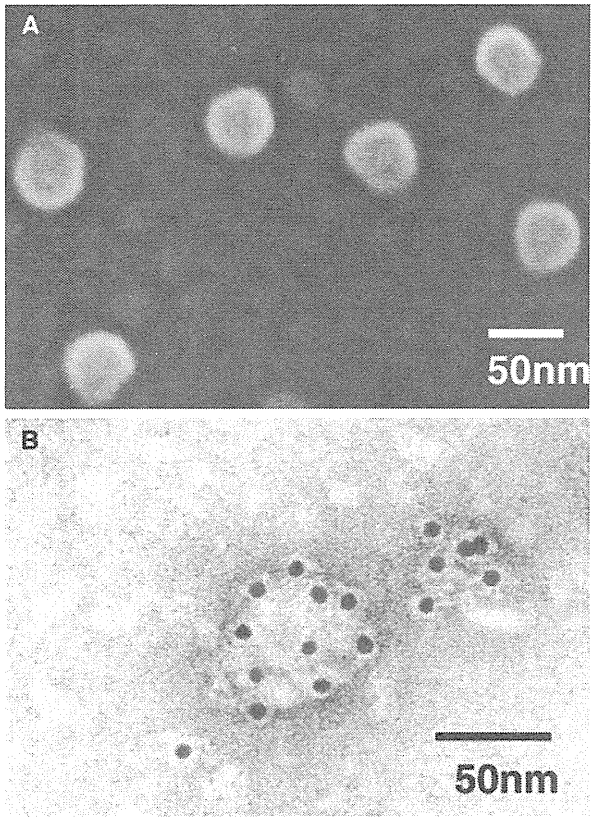

Fig. 3 Electron microscopy analysis of virus-like particles. The core-protein-rich fraction collected from the density gradient was further concentrated by ultracentrifugation and observed by scanning electron microscopy (A). The same fraction attached to formvar-coated grids was incubated with rabbit anti-E2 RR6 antibody, treated with goat anti-rabbit IgG coupled to 10-nm colloidal gold, negatively stained with uranyl acetate, and then examined by transmission electron microscopy (B)

out with full-genome replicon cells produced no infectivity in the supernatant (data not shown). Under the most efficient conditions, the titer of the supernatant reached as high as 20 cfu (colony-forming units) per milliliter when the putative doubling time of these cells was approximately 24 h. Furthermore, the appearance of colonies was abolished by addition of the antibody JS-81 (BD Pharmingen), an antibody to CD81, a possible co-receptor of HCV [22] (Fig. 4B).

Next, we propagated some of these colonies for further analysis. Northern blot analysis showed that these clones carry HCV RNAs of reasonable size (Fig. 5A), including subgenomic RNA (7994 bases), dORF RNA (10994 bases), and dORF bla RNA (11840 bases). Western blot analysis revealed that the cell clones that were infected with supernatant from Huh-7 cells containing the dORF replicon expressed structural proteins (Fig. 5B), indicating that the colonies were not just the reappearance of subgenomic replicons hidden in the cured cells.

Together, our findings indicate that these particles in the supernatant infected the Huh-7 cells through a CD81-associated pathway and that infected cells formed colonies after G418 selection, similar to what was observed with electroporation with subgenomic RNA.

A reporter gene inserted into the dORF replicon RNA can be transmitted through infection

First, we confirmed that the beta-lactamase gene in the dORF bla replicon RNA was active in established replicon cell clones and able to process the green fluorescent substrate into blue fluorescent product (Fig. 6A). Next, we attempted to detect the activity of the beta-lactamase gene in the cloned infected colonies. Three clones grown from cells infected with the dORF bla supernatant were treated using a GeneBLAzer In Vivo Detection Kit. One clone was positive for blue fluorescence (Fig. 6B), demonstrating that a reporter gene inserted into the dORF replicon could be transmitted to naive Huh-7 cells through secreted virus particles in the culture supernatant.

Discussion

There have been several previous reports of full-genome HCV replicons that can replicate well in Huh-7 cells and express sufficient amounts of structural proteins [1, 4, 7, 14, 20]. Pietschmann et al. (2002) observed the secretion of an RNase-resistant HCV genome into the supernatant from both full-genome and subgenomic replicon cells and non-specific uptake of these genomes by naive Huh-7 cells. Ikeda et al. (2002) were also unable to detect any infectivity in the supernatant of their full-genome replicon cells. They assumed that the reason for this failure was the inability of Huh-7 cells to release intact virions or to be infected by the virus, although this was later demonstrated not to be the case by a series of reports on infection using the JFH-1 clone [16, 26, 30].

First, we attempted to improve the efficiency of the full-genome replicon in two ways, namely, by modifying the construct and reducing the genome size. Numerous studies have examined the encapsidation signal in the genomic RNA of positive-sense single-stranded viruses [5, 8, 9]. Frolova et al. [5] showed that the encapsidation signal of Sindbis virus lies in the nsP1 gene and is 132 nucleotides long. Johansen et al. [9] found that the IRES of poliovirus had the ability to enhance the efficiency of packaging of the polio subgenomic replicon. We think that these findings indicate that the construction of the genome could affect the efficacy of encapsidation, and we therefore decided to

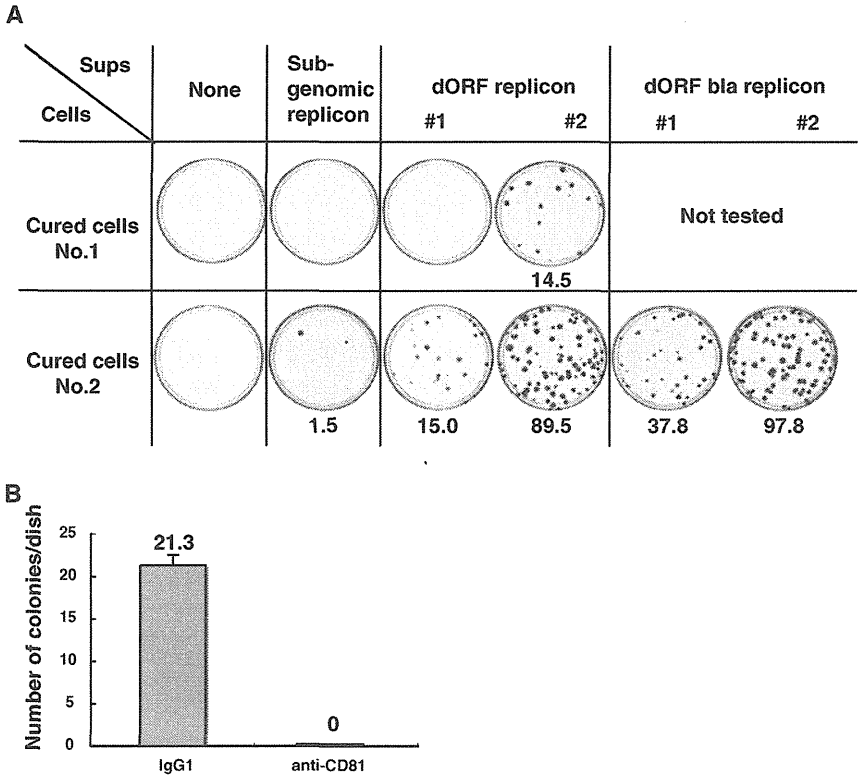

Fig. 4 Infectivity of supernatants from various replicon cells. Colonies of cells infected with the indicated supernatant. Numbers shown below the plates are the average of a total of four plates per condition (A). Inhibition of infection by anti-CD81 antibody. Cured cell K4 cells (No.2 in Fig. 4A) were treated with mouse IgG1 as the negative control or anti-CD81 before infection (B)

change the site of genome division from the beginning of the core region to the middle of the NS2 region. Regarding the size of the genome, there have been reports that the insertion of a foreign gene of significant size can result in the deletion of a portion of the chimeric genome during replication [18, 19]. We therefore removed the second half of the NS2 region, because this region appears to be unnecessary for both replication and packaging in Huh-7 cells, and this deletion was found to have no influence on the efficacy of encapsidation, as there were no apparent differences between the NS2-deleted construct and the one containing the entire NS2 region (data not shown).

Our established dORF replicon was able to replicate well in Huh-7 cells and express sufficient amounts of structural proteins, similar to the previously reported full-genome replicon. Although both the dORF replicon cells and the previously reported full-genome replicons secreted RNase-resistant genomes, there was a striking difference between these two full-genome replicons when NP-40 treatment was carried out on their supernatants. There was no RNase-resistant genome left in the NP-40-treated supernatant of full-genome replicons, although density gradient analysis of the NP-40-treated supernatant of dORF replicon cells clearly showed the coexistence of the HCV genome and core proteins at a peak of 1.18 g/mL. This peak may represent NP-40-resistant nucleocapsids. The distribution of core proteins in the density gradient analysis of the concentrated supernatant of the dORF replicons did not match that of the HCV genome. A reasonable explanation for this mismatch is that the lighter side of the broad peak of the HCV genome was not representative of intact virions and is instead an indication of secretion by a pathway used in subgenomic replicon cells, which differs from the natural process. The fact that the peak of the HCV genome of full-genome replicons was located in a narrow range on the lighter side compared to that of the dORF replicons supports this hypothesis. We observed round particles in the concentrated core protein fraction using electron microscopy, and those particles also seemed to contain core proteins. These findings indicate that our dORF replicon cells produced both intact virions and artificial membranous particles, with the former having the morphological and biophysical characteristics of putative virions.

The colony-forming assay clearly demonstrated the ability of the supernatants of our dORF replicon cells to infect Huh-7 cells efficiently. The reason for the difference in efficacy between the two cured cells is uncertain but may involve the ability to support replication or the level of receptor expression. This needs to be clarified in order to improve the efficiency of HCV infection in vitro. Differences in the efficiency of infection were also noted between

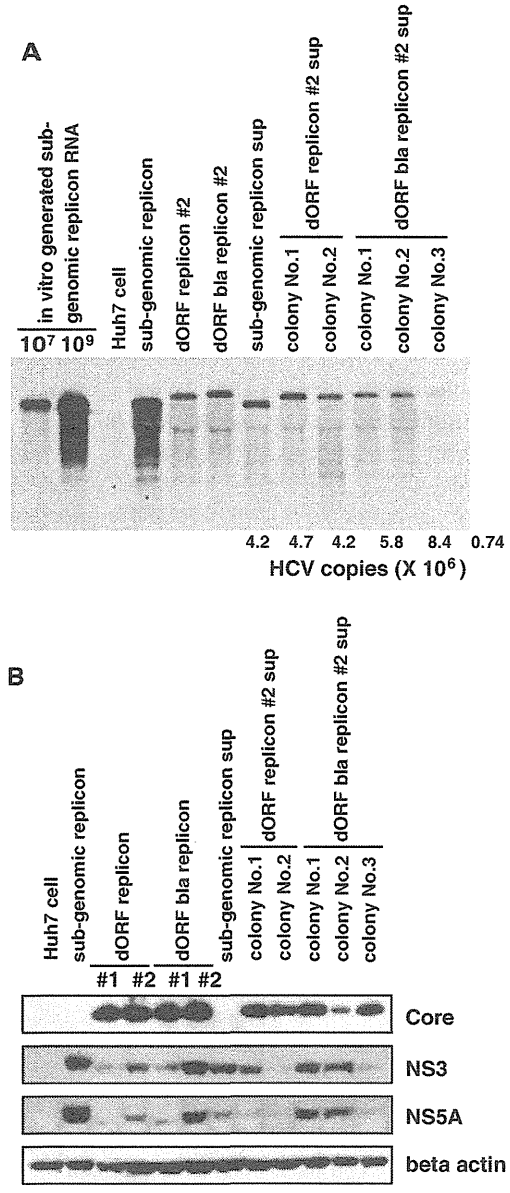

Fig. 5 Northern blot analysis of colonies formed after infection. 10^7, 10^9: amounts of in vitro-generated subgenomic replicon RNA loaded. Numbers below the lanes are the HCV copy number per μg of total RNA (A). Huh-7 cells, subgenomic replicon cells, dORF replicon cell #2, dORF bla replicon cell #2, subgenomic replicon sup: colony from cells transduced with subgenomic replicon supernatant, colony No.1, 2 of dORF replicon #2 sup: colonies from cells infected with dORF replicon #2 supernatant, colony No.1, 2, and 3 of dORF bla replicon #2 sup: colonies from cells infected with dORF bla replicon #2 supernatant. Western blot analysis of colonies formed after infection (B). The order of the lanes is identical to that for the northern blot, except for the dORF and dORF bla replicons, which represent two clones in this figure

clones of the same dORF replicon cells, which may have been due to the accumulation of different mutations in the structural region, although we have not yet confirmed this

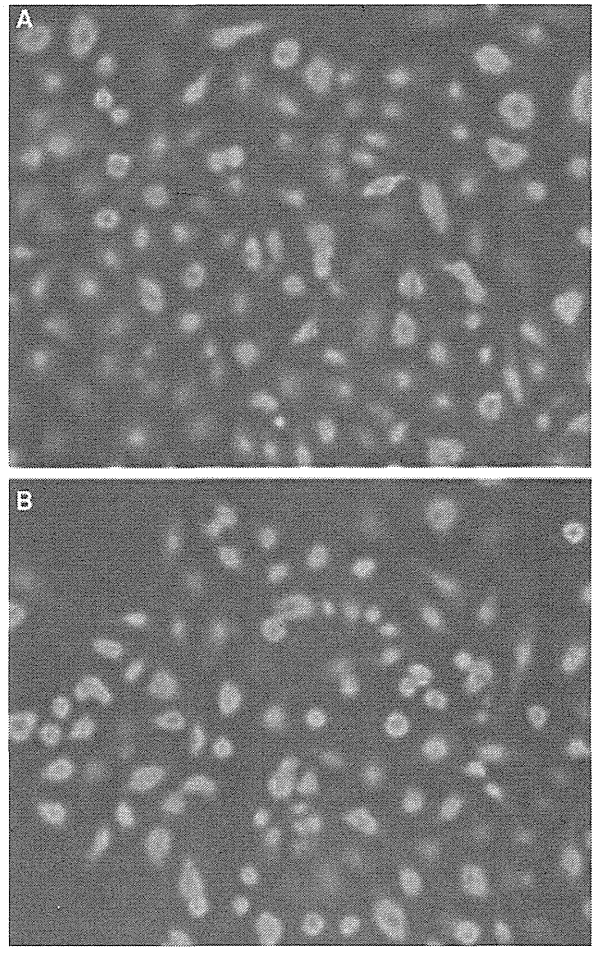

Fig. 6 Detection of beta-lactamase activity in dORF replicon cells. Parental dORF bla replicon #2 cell (A) and colony no. 3 cloned from cells infected with dORF bla replicon #2 cell supernatant (B). Blue fluorescence shows high beta-lactamase activity, indicating that the reporter gene functioned normally after infection

hypothesis. We also observed colonies being formed by cells that were treated with supernatant containing subgenomic replicons, and these colonies most likely represent the so-called "non-specific transduction" of the subgenomic replicon. Although this dORF supernatant infection could be blocked by the anti-CD81 antibody reported previously [30], we cannot exclude the possibility that the infection we observed was due to highly efficient "non-specific transduction," as we could not determine whether "non-specific transduction" also could be affected by the anti-CD81 antibody because of the low colony-forming ability of the supernatant of subgenomic replicons.

We also demonstrated that the reporter gene that was inserted in addition to the neomycin resistance gene could be transmitted to the new generation of viruses. This finding raises the possibility of producing sufficient amounts of reporter virus constitutively.

In summary, we established an infectious-particle-producing HCV replicon system. This achievement should yield more precise information about the encapsidation signal of HCV, which was kept intact despite the partitioning of the genome. This system also allows analysis of the pathway of HCV infection, including adsorption of virions to cell-surface receptors, penetration, uncoating, virus particle assembly, and HCV release. Moreover, the dORF replicon system may be used as a convenient tool to investigate the utility of the newly established siRNA system [14, 27] and evaluation of compounds that are effective against subgenomic replicons.

Although we believe that the reason for our success is our new construct, further examination is necessary to verify our findings.

Materials and methods

Construction and RNA transcription

To construct dORF replicon RNA, the second half of the NS2 region of the HCV-R6 strain [25] was replaced in frame with the foot and mouth disease virus (FMDV) 2A protease gene, the neomycin resistance gene, and the encephalomyocarditis virus (EMCV) internal ribosomal entry site (IRES). In addition, the region from NS3 to the beginning of NS5B was replaced with the 1bneo/delS replicon sequence from the N strain of genotype 1b [6](kindly provided by Dr. Seeger). This construct was designated as the "divided open reading frame carrying full genome" (dORF) replicon. The subgenomic replicon construct was also prepared from the R6 strain and also contained the 1bneo/delS replacement. For the reporter assay, the FMDV 2A protease gene and beta-lactamase gene (bla; Invitrogen) were inserted after the remaining NS2 gene to produce the dORF bla replicon construct. Replication-deficient versions of these three replicons were also prepared by deleting 27 nucleotides, including the GDD motif of NS5B polymerase.

In vitro transcription of these replicon RNAs was performed using the MEGAscript kit (Ambion).

Cell culture and electroporation

Huh-7 cells were cultured in DMEM (SIGMA) with 10% fetal bovine serum. Replicon cells were maintained in the same medium supplemented with 300 μg/mL G418 (Invitrogen). These cells were passaged 3 times a week at a 4:1 splitting ratio. Electroporation of replicon RNA was performed as described previously [17]. The subgenomic replicon (1bneo/delS replicon) cells were treated with 1000 IU of IFN-α for 2 months and cloned by the limited dilution method. Two of these clones were designated as HCV replicon-cured Huh-7 cells F2 and K4. The cell line containing the full-genome replicon of genotype1b, namely the NNC#2 clone [15], was a kind gift from Dr. Shimotohno of Keio University.

Northern blot analysis and quantification of HCV RNA

Total RNA was purified from cells using ISOGEN (Nippon Gene) for northern blot analysis or ABI prizm6100 (Applied Biosystems) for real-time RT-PCR. Purified RNAs were quantified by absorbance at 260 nm. For northern blot analysis, 30 μg of each total RNA was used with a Northern Max Kit (Ambion) according to the manufacturer's instructions. The probe for detection of HCV RNA was a PCR fragment of the NS5B region (nucleotide numbers 7629–7963) that had been biotin-labeled using a BrightStar Psoralen-Biotin Kit (Ambion) according to the manufacturer's instructions. Following hybridization of the membranes, the probe was detected using a BrightStar BioDetect Kit (Ambion) according to the manufacturer's instructions, and luminescence was detected using the LAS1000 detection system (Fujifilm). Measurement of the HCV RNA copy number by real-time RT-PCR was performed using an ABI PRISM 7900 system (Applied Biosystems) as described previously [24].

Western blot analysis

Western blot analysis was carried out using the conventional semi-dry blot method. Cells were lysed with buffer containing 100 mM Tris-HCl (pH 7.4) and 4% sodium dodecyl sulfate. A 10-μg amount of protein from each sample was separated by SDS-PAGE through a 4–20% gradient gel (Invitrogen) and transferred to the membrane according to the gel manufacturer's protocol. The antibodies used in this study were anti-core mouse monoclonal antibody (MAb), anti-E1 MAb, anti-E2 MAb (reported previously; [25]), anti-NS3 antiserum (reported previously; [25]), anti-NS5B antiserum (Upstate), and anti-beta-actin MAb (Abcam). Horseradish peroxidase-labeled anti-mouse and anti-rabbit IgG goat antibodies (Santa Cruz Biotechnology and DAKO, respectively) were used as the secondary antibody. The membranes were treated using an ECL Plus kit (Amersham) according to the manufacturer's instructions, and luminescence was detected using an LAS1000 system (Fujifilm).

Density gradient analysis and core ELISA

Culture supernatants from replicon cells were loaded onto 10–60% sucrose density gradient tubes with or without 10-fold concentration in an Amicon-100 (Millipore). The

tubes were then ultracentrifuged at 100,000 *g* for 16 h and fractionated. NP-40 was added to the culture supernatants to a final concentration of 0.5%, and they were then incubated at 4°C for 30 min. For electron microscopy, the culture supernatant was concentrated, loaded onto a 60% sucrose cushion, and ultracentrifuged at 100,000 *g* for 4 h. The interface between the concentrated medium and the sucrose cushion was collected and separated by the density gradient method described above. A 2-mL fraction from 5 ml to 7 mL from the bottom, with a density of 1.1–1.2 g/mL, was examined by electron microscopy after further concentration by the sucrose cushion ultracentrifugation method described above. The amount of core protein in the fractions was quantified using an Ohso ELISA kit in accordance with the manufacturer's instructions.

Electron microscopy

The concentrated fraction of core protein was observed by scanning and transmission electron microscopy. For scanning electron microscopy, the sample was allowed to settle on the surface of a poly-L-lysine-coated glass cover slip for 30 min, and the attached sample was then fixed with 0.1% glutaraldehyde in 0.1 M phosphate buffer (pH 7.4) for 10 min, washed three times with 0.1 M phosphate buffer, and post-fixed with 1% osmium tetroxide in the same buffer for 10 min. After dehydration through a graded series of ethanol, the samples were dried in a freeze dryer (Hitachi ES-2020, Hitachi) using t-butyl alcohol, coated with osmium tetroxide, approximately 2 nm thick, using an osmium plasma coater (NL-OPC80; Nippon Laser and Electronics Laboratory), and then examined using a Hitachi S-4800 field emission scanning electron microscope at an accelerating voltage of 10 kV [23]. For transmission electron microscopy, the sample was allowed to settle on a formvar-coated nickel grid for 10 min, dried in air, incubated with rabbit anti-E2RR6 antibody (prepared as described in the supplementary information), washed with PBS, and then incubated with goat anti-rabbit IgG coupled to 10-nm colloidal gold (British BioCell). After negative staining with 2% uranyl acetate, the sample was examined using a JEM 1200EX transmission electron microscope (JEOL) at an accelerating voltage of 80 kV.

Rabbit anti-E2 RR6 antibody to the HCV-E2 protein was prepared as follows: The E2 gene of HCV type 1b [25] was cloned under the control of the ATI-P7.5 hybrid promoter of vaccinia virus vector pSFB4 and allowed to recombine with the Lister strain of the vaccinia virus to give vector RVV. Rabbits were infected intradermally with 10^8 p.f.u. of RVV, and 2 months later, they received two booster injections with the purified E2 protein. HCV-E2 protein was expressed from the RVV vector and purified by lentil lectin column chromatography and affinity chromatography using an anti-E2 monoclonal antibody [25].

Infection

A 2.5-ml aliquot of cleared culture supernatants from replicon cells was added to approximately 70% confluent of Huh-7 cells in 25-cm^2 flasks, and the same amount of complete DMEM was added 2 h later. Infected cells were transferred to 75-cm^2 flasks the next day and to four 10-cm dishes 2 days later. G418 at a concentration of 300 μg/mL was added to the medium immediately after the second passage. The three types of Huh-7 cells used in this study included the one purchased from J.C.R.B. and the 2 IFN-cured replicon cell lines F2 and K4 described above. The medium was changed every other day. For the blocking experiment, cells were treated with the anti-CD81antibody as described previously [30]. Cells were fixed with 10% formalin/PBS(-) for 10 min after washing with PBS(-) and staining with 1% crystal violet/PBS(-) for 1 h before washing with water.

Beta-lactamase detection assay

Beta-lactamase activity was detected using a GeneBLAzer In Vivo Detection Kit (Invitrogen) according to the manufacturer's instructions and observed using a fluorescence microscope (Nikon) with UV light excitation.

Acknowledgments The authors would like to thank Dr. Christoph Seeger of the Fox Chase Cancer Center for providing the 1bneo/delS replicon plasmid and Dr. Kunitada Shimotohno of Keio University for providing full-genome genotype 1b replicon clone NNC#2. We also thank Etsuko Endo for her secretarial work and Dr. Masahiro Shuda for fruitful discussions. This study was supported in part by grants from the Ministry of Education, Culture, Sports, Science and Technology of Japan, the Program for Promotion of Fundamental Studies in Health Sciences of the National Institute of Biomedical Innovation of Japan, and the Ministry of Health, Labour and Welfare of Japan.

References

1. Blight KJ, McKeating JA and Rice CM (2002) Highly permissive cell lines for subgenomic and genomic hepatitis C virus RNA replication. J Virol 76:13001-13014
2. Choo QL, Kuo G, Weiner AJ, Overby LR, Bradley DW and Houghton M (1989) Isolation of a cDNA clone derived from a blood-borne non-A, non-B viral hepatitis genome. Science 244:359-362
3. Date T, Kato T, Miyamoto M, Zhao Z, Yasui K, Mizokami M and Wakita T (2004) Genotype 2a hepatitis C virus subgenomic

replicon can replicate in HepG2 and IMY-N9 cells. J Biol Chem 279:22371-6
4. Date T, Miyamoto M, Kato T, Morikawa K, Murayama A, Akazawa D, Tanabe J, Sone S, Mizokami M and Wakita T (2007) An infectious and selectable full-genome replicon system with hepatitis C virus JFH-1 strain. Hepatol Res 37:433-443
5. Frolova E, Frolov I and Schlesinger S (1997) Packaging signals in alphaviruses. J Virol 71:248-258
6. Guo J, Bichko VV and Seeger C (2001) Effect of alpha interferon on the hepatitis C virus replicon. J Virol 75:8516-8523
7. Ikeda M, Yi M, Li K and Lemon SM (2002) Selectable subgenomic and genome-length dicistronic RNAs derived from an infectious molecular clone of the HCV-N strain of hepatitis C virus replicate efficiently in cultured Huh7 cells. J Virol 76:2997-3006
8. Jia X-Y, Van Eden M, Busch MG, Ehrenfeld E and Summers DF (1998) Trans-encapsidation of a poliovirus replicon by different picornavirus capsid proteins. J Virol 72:7972-7977
9. Johansen LK and Morrow CD (2000) The RNA encompassing the internal ribosome entry site in the poliovirus 5′ nontranslated region enhances the encapsidation of genomic RNA. Virology 273:391-399
10. Kanda T, Basu A, Steele R, Wakita T, Ryerse JS, Ray R and Ray RB (2006) Generation of infectious hepatitis C virus in immortalized human hepatocytes. J Virol 80:4633-4639
11. Kanto T, Hayashi N, Takehara T, Hagiwara H, Mita E, Naito M, Kasahara, A, Fusamoto H and Kamada T (1994) Buoyant density of hepatitis C virus recovered from infected hosts: two different features in sucrose equilibrium density-gradient centrifugation related to degree of liver inflammation. Hepatology 19:296-302
12. Kato T, Furusaka A, Miyamoto M, Date T, Yasui K, Hiramoto J, Nagayama K, Tanaka T and Wakita T (2001) Sequence analysis of hepatitis C virus isolated from a fulminant hepatitis patient. J Med Virol 64:334-339
13. Kato T, Date T, Miyamoto M, Furusaka A, Tokushige K, Mizokami M and Wakita, T (2003) Efficient replication of the genotype 2a hepatitis C virus subgenomic replicon. Gastroenterology 125:1808-1817.
14. Kim M, Shin D, Kim SI and Park M (2006) Inhibition of hepatitis C virus gene expression by small interfering RNAs using a tricistronic full-length viral replicon and a transient mouse model. Virus Res 122:1-10
15. Kishine H, Sugiyama K, Hijikata M, Kato N, Takahashi H, Noshi T, Nio Y, Hosaka M, Miyanari Y, Shimotohno K (2002) Subgenomic replicon derived from a cell line infected with the hepatitis C virus. Biochem Biophys Res Commun 293:993-9
16. Lindenbach BD, Evans MJ, Syder AJ, Wolk B, Tellinghuisen TL, Liu C C, Maruyama T, Hynes RO, Burton DR, McKeating JA and Rice CM (2005) Complete replication of hepatitis C virus in cell culture. Science 309:623-626
17. Lohmann V, Korner F, Koch J, Herian U, Theilmann L and Bartenschlager R (1999) Replication of subgenomic hepatitis C virus RNAs in a hepatoma cell line. Science 285:110-113
18. Lu, HH, Alexander L and Winner E (1995) Construction and genetic analysis if dicistronic Polioviruses containing open reading frames for epitopes of Human Immunodeficiency Virus type 1 gp120. J Virol 69:4797-4806
19. Mattion NM, Reilly PA, DiMichele SJ, Crowley JC and Weeks-Levy C (1994) Attenuated poliovirus strain as a live vector: expression of regions of rotavirus outer capsid protein VP7 by using recombinant Sabin 3 viruses. J Virol 68:3925-3933
20. Pietschmann T, Lohmann V, Kaul A, Krieger N, Rinck G, Rutter G, Strand D and Bartenschlager R (2002) Persistent and transient replication of full-length hepatitis C virus genomes in cell culture. J Virol 76:4008-4021
21. Pietschmann T, Kaul A, Koutsoudakis G, Shavinskaya A, Kallis S, Steinmann E, Abid K, Negro F, Dreux M, Cosset FL and Bartenschlager R (2006) Construction and characterization of infectious intragenotypic and intergenotypic hepatitis C virus chimeras. Proc Natl Acad Sci USA 103:7408-7413
22. Pileri P, Uematsu Y, Campagnoli S, Galli G, Falugi F, Petracca R, Weiner AJ, Houghton M, Rosa D, Grandi G and Abrignani S (1998) Binding of hepatitis C virus to CD81. Science 282:938-941
23. Suzuki H, Murasaki K, Kodama K and Takayama H (2003) Intracellular localization of glycoprotein VI in human platelets and its surface expression upon activation. Bri J Haematol 121:904-912
24. Takeuchi T, Katsume A, Tanaka T, Abe A, Inoue K, Tsukiyama-Kohara K, Kawaguchi R, Tanaka S and Kohara M (1999) Real-time detection system for quantification of hepatitis C virus genome. Gastroenterology 116:636-42
25. Tsukiyama-Kohara K, Tone S, Maruyama I, Inoue K, Katsume A, Nuriya H, Ohmori H, Ohkawa J, Taira K, Hoshikawa Y, Shibasaki F, Reth M, Minatogawa Y and Kohara M (2004) Activation of the CKI-CDK-Rb-E2F pathway in full genome hepatitis C virus-expressing cells. J Biol Chem 279:14531-14541
26. Wakita T, Pietschmann T, Kato T, Date T, Miyamoto M, Zhao Z, Murthy K, Habermann A, Krausslich HG, Mizokami M, Bartenschlager R and Liang TJ (2005) Production of infectious hepatitis C virus in tissue culture from a cloned viral genome. Nat Med 11:791-796
27. Watanabe T, Sudoh M, Miyagishi M, Akashi H, Arai M, Inoue K, Taira K, Yoshiba M and Kohara M (2006) Intracellular-diced dsRNA has enhanced efficacy for silencing HCV RNA and overcomes variation in the viral genotype. Gene Ther 13:883-92
28. Yi MK and Lemon SM (2004) Adaptive mutations producing efficient replication of genotype 1a Hepatitis C virus RNA in normal Huh7 cells. J Virol 78:7904-7915
29. Yi MK, Villanueva RA, Thomas D, Wakita T and Lemon SM (2006) Production of infectious genotype 1a hepatitis C virus (Hutchinson strain) in cultured human hepatoma cells. Proc Natl Acad Sci USA 103:2310-2315
30. Zhong J, Gastaminza P, Cheng G, Kapadia S, Kato T, Burton DR, Wieland SF, Uprichard SL, Wakita T and Chisari FV (2005) Robust hepatitis C virus infection in vitro. Proc Natl Acad Sci USA 102:9294-9299

JLB

Article

Role of interleukin-18 in intrahepatic inflammatory cell recruitment in acute liver injury

Kiminori Kimura,*,†,1 *Satoshi Sekiguchi*,† *Seishu Hayashi*,* *Yukiko Hayashi*,‡ *Tsunekazu Hishima*,‡ *Masahito Nagaki*,§ *and Michinori Kohara*†

Divisions of *Hepatology and ‡Pathology, Tokyo Metropolitan Cancer and Infectious Diseases Center, Komagome Hospital, Tokyo, Japan; †Department of Microbiology and Cell Biology, Tokyo Metropolitan Institute of Medical Science, Tokyo, Japan; and §Department of Gastroenterology, Gifu University Graduate School of Medicine, Gifu, Japan

RECEIVED JULY 20, 2010; REVISED OCTOBER 12, 2010; ACCEPTED NOVEMBER 9, 2010. DOI: 10.1189/jlb.0710412

ABSTRACT

Although the innate immune system has been demonstrated to play important roles as the first line of defense against various infections, little is known about the interactions between intrahepatic inflammatory cells and the cytokine network in the liver. Here, we examined the role of IL-18 in IHL recruitment in acute liver injury. C57BL/6 mice were injected with an αCD40 mAb, and their serum IL-18 levels were observed to increase, with subsequent recruitment of IHLs into the liver. NKT cells were involved in this liver injury, as the serum ALT levels were reduced in NKT KO mice through the suppression of macrophage and monocyte migration and cytokine production. In contrast, depletion of neutrophils exacerbated the liver injury associated with high levels of TNF-α and IL-18 and increased numbers of macrophages and monocytes. Treatment with a neutralizing antibody against IL-18 reduced the serum ALT levels and inflammatory cell accumulation in the liver. Finally, additional administration of rIL-18 with αCD40 injection caused severe liver injury with increased IFN-γ production by NK cells. In conclusion, these findings demonstrate that IL-18 modulates liver inflammation by the recruitment of inflammatory cells, including NKT cells, macrophages, monocytes, and neutrophils. *J. Leukoc. Biol.* 89: 433–442; 2011.

Introduction

Macrophages of the innate immune system are the first line of defense against many pathogens and play a crucial role in the elimination of bacterial infections [1]. The resident liver macrophages, Kupffer cells, are well known to be phagocytic macrophages and account for 80% of the total population of fixed tissue macrophages in the body [2]. These cells are derived from blood monocytes and found mainly in the hepatic sinusoid [3]. They are continuously exposed to various pathogenic components, such as the gram-negative bacteria cell wall constituent LPS, and have the ability to protect their host immediately from the associated bacteria. Activated macrophages can also secrete inflammatory cytokines, such as TNF-α, IL-12, IL-18 [4, 5], and chemokines [6], in response to certain stimuli. These mediators produced by macrophages and the capacity for phagocytosis are essential for protection against microorganisms [7].

In contrast, NKT cells express an invariant TCR chain (V14-J281 in mice) and recognize glycolipid antigens, such as α-galactosylceramide, in association with the MHC class I-like molecule CD1d [8]. APCs, including DCs and macrophages, present antigens to NKT cells, a process that is dependent on CD40 ligation and results in the rapid release of large amounts of Th1 and Th2 cytokines and chemokines. Activated NKT cells can also provide maturation signals for other inflammatory cells, especially DCs, NK cells, and macrophages, thereby involving innate and acquired immunity [9, 10].

IL-18 is a member of the IL-1 family that is produced as a biologically inactive precursor and secreted after activation by cleavage with caspase-1 or other caspases [11]. Originally, IL-18 was identified as an IFN-γ-inducing factor that can act on Th1 cells, nonpolarized T cells, NK cells, B cells, and DCs to produce IFN-γ in the presence of IL-12 [12]. Besides its potent induction of IFN-γ, IL-18 activates NK and T cells, which play central roles in viral clearance [13].

We have already demonstrated that αCD40 mAb injection induces biphasic liver injury by way of inflammatory cytokine and chemokine production [14]. Furthermore, this liver injury requires NK cells and macrophages in the early-phase events, and B cells also contribute to the late-phase liver inflammation [15]. During analyses of this liver injury model, we found that

Abbreviations: αCD40=anti-CD40, ALT=alanine aminotransferase, IHL=intrahepatic leukocyte, KO=knockout (deficient), NLR=NOD-like receptor

The online version of this paper, found at www.jleukbio.org, includes supplemental information.

1. Correspondence: Division of Hepatology, Tokyo Metropolitan Cancer and Infectious Diseases Center, Komagome Hospital, 18-22-3 Honkomagome, Bunkyo-ku, Tokyo 113-8677, Japan. E-mail: kkimura@cick.jp

serum IL-18 was increased dramatically at the late phase. In the present study, we investigated the involvement of IL-18 in the liver injury and focused on the interactions among IL-18 and NKT cells, neutrophils, macrophages, and monocytes, which play important roles in various diseases. The results obtained provide new insights into the inflammatory network among macrophages, neutrophils, and NKT cells during liver injury.

MATERIALS AND METHODS

Mice

Vα14 NKT KO mice were generated as described [7], and C57BL/6 mice were purchased from Japan SLC (Shizuoka, Japan). All animals were housed in pathogen-free rooms under strict barrier conditions and received humane care according to the guidelines of the Animal Care Committees of Gifu University School of Medicine (Gifu, Japan) and Tokyo Metropolitan Institute of Medical Science (Tokyo, Japan).

Antibodies

Mice were injected i.v. with 100 μg αCD40 [16] or 100 μg purified rat IgG2a as a control (BD PharMingen, San Diego, CA, USA). In addition, some mice were injected i.p. (200 μg/mouse) at Days −1, +1, and +3 with a rat mAb against mouse Gr-1 (clone RB6-8C5) and control rat IgG2b (both from eBioscience, San Diego, CA, USA). At Days −1, +1, and +3, other mice were injected i.p. with a rat anti-mouse IL-18 mAb (50 μg/mouse) and rat IgG (both from MBL, Nagoya, Japan).

Cell isolation

To isolate IHLs, single-cell suspensions were prepared from liver perfused with PBS via the inferior vena cava and digested in 10 mL RPMI 1640 (Life Technologies, Gaithersburg, MD, USA) containing 0.02% (wt/vol) collagenase IV (Sigma-Aldrich, St. Louis, MO, USA) and 0.002% (wt/vol) DNase I (Sigma-Aldrich) for 40 min at 37°C. Cells were overlaid on Lympholyte M (Cedarlane, Westbury, NY, USA) in PBS. Bone marrow cells were collected from the femurs and tibias of mice. To isolate PBMCs, peripheral blood (0.4 mL) was obtained by cardiac puncture under ether anesthesia. After density separation, cell counts and immunofluorescence analyses were performed.

Tissue RNA analyses

Frozen livers were mechanically pulverized under liquid nitrogen, and total RNAs were isolated for RPAs as described previously [15]. All reagents for the RPAs were purchased from BD PharMingen.

ELISA

The serum IL-18, TNF-α, and IFN-γ concentrations were assayed using specific ELISA kits (IL-18, MBL; TNF-α and IFN-γ, Genzyme Techne Corp., Minneapolis, MN, USA), according to each corresponding manufacturer's protocols.

Immunohistochemistry

The samples were embedded in OCT compound (Tissue Tek, Miles, Elkhart, IN, USA) and frozen in liquid nitrogen. Sections were cut at 4 μm thickness using a cryostat and fixed with cold acetone for 10 min. The fixed sections were treated with rat anti-mouse F4/80, Ly-6C, and Gr-1 mAb (10 μg/mL), followed by a streptavidin-biotin-HRP complex (Dako, Glostrup, Denmark). The positive reactions were visualized with 0.035% H_2O_2 and 0.03% 3,3′-diaminobenzidine (Wako, Tokyo, Japan) in 50 mM Tris-HCl (pH 7.6) for 2–3 min. After 4% formaldehyde fixation, the stained sections were counterstained with hematoxylin and subjected to microscopic observation.

Flow cytometry

The cells were surface-stained with fluorochrome-conjugated mAb for 20 min on ice. The following antibodies were used: anti-CD3, anti-NK1.1, anti-CD11b, and anti-CD11c (all from eBioscience). The F4/80 and Ly-6C mAb (BMA Biomedicals, Geneva, Switzerland) were also used. In addition, the cells were surface-stained with FITC-conjugated anti-CD3, FITC-conjugated anti-CD11b, and allophycocyanin-conjugated anti-NK1.1 mAb, together with anti-IFN-γ-PE and anti-TNF-α-PE mAb (all from BD PharMingen) for intracellular cytokine detection. Samples were acquired using a FACSCalibur flow cytometer, and data were analyzed using the CellQuest software (BD Immunocytometry Systems, San Jose, CA, USA) and FlowJo software (Tree Star, San Carlos, CA, USA).

BrdU incorporation

For in vivo BrdU labeling, mice received a 100-μL i.p. injection of a 10-mg/mL solution of BrdU in PBS at 2 h before sacrifice. Single-cell suspensions of IHLs were prepared at 24 h after αCD40 injection and surface-stained with PE-CD11b. Following the surface staining, the cells were fixed, stained for intracellular BrdU using a FITC-BrdU flow kit (BD PharMingen), and analyzed by flow cytometry.

Data analysis

All data are expressed as the mean + SD. Values of $P < 0.05$ were considered statistically significant.

RESULTS

A single injection of αCD40 increases serum IL-18

We found that the serum ALT activity began to elevate on Day 1 and was clearly increased on Day 5 after αCD40 injection. We confirmed further that inflammatory cytokine and chemokine mRNA expressions were increased at Days 1 and 5 in C57BL/6 mice (Supplemental Fig. 1A). We measured the serum IL-18 level and found that it began to increase at Day 3 and was remarkably increased until Day 5 after the injection. To determine the infiltration of inflammatory cells in the same livers, we counted the absolute number of IHLs and calculated the number of cells in each IHL subset. As shown in **Fig. 1B**, Gr-1^{++}/CD$11b^{+}$ cells (mostly neutrophils) were increased until Day 1 and then decreased at Days 3 and 5. On the other hand, Gr-1^{+}/CD$11b^{+}$ cells (mostly macrophages and monocytes) were increased and reached a peak at Day 3 and then decreased until Day 5. Furthermore, to evaluate the numbers of macrophages and their precursors in the liver, the cells were stained with the CD11b, F4/80, and Ly-6C mAb, which recognize antigens on macrophages and their precursors at different stages of differentiation [17]. The numbers of Ly-$6C^{++}$/CD$11b^{+}$ cells (mostly monocytes) and F4/80^{+}/CD$11b^{+}$ cells (tissue macrophages) began to increase by Day 1, reached a peak at Day 3, and then decreased until Day 5. In immunohistochemical analyses, Gr-1^{+} cells were increased at Day 1 in the liver parenchyma, whereas Ly-$6C^{+}$ and F4/80^{+} cells were increased at Day 3 in the liver (Fig. 1C), consistent with the FACS data.

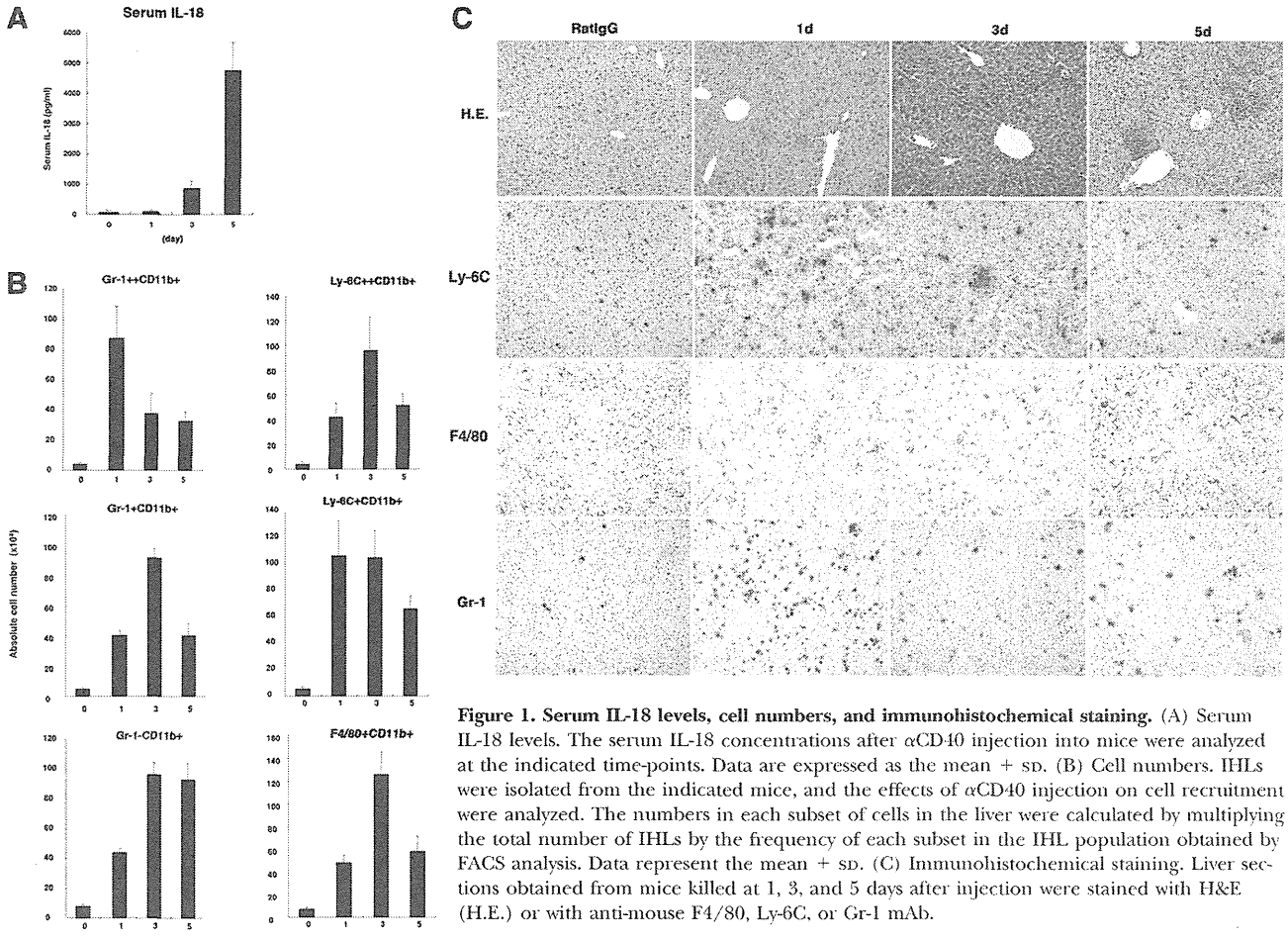

Figure 1. Serum IL-18 levels, cell numbers, and immunohistochemical staining. (A) Serum IL-18 levels. The serum IL-18 concentrations after αCD40 injection into mice were analyzed at the indicated time-points. Data are expressed as the mean + SD. (B) Cell numbers. IHLs were isolated from the indicated mice, and the effects of αCD40 injection on cell recruitment were analyzed. The numbers in each subset of cells in the liver were calculated by multiplying the total number of IHLs by the frequency of each subset in the IHL population obtained by FACS analysis. Data represent the mean + SD. (C) Immunohistochemical staining. Liver sections obtained from mice killed at 1, 3, and 5 days after injection were stained with H&E (H.E.) or with anti-mouse F4/80, Ly-6C, or Gr-1 mAb.

Proliferation and differentiation of macrophages after αCD40 injection

As reported previously [14], macrophages were key players in this liver injury. We confirmed that αCD11b mAb treatment suppressed inflammatory cytokine and chemokine expressions in the liver and the serum IL-18 levels (Supplemental Fig. 2A and B), indicating that macrophages are IL-18 producers, consistent with a previous report [11].

Next, to evaluate the function of macrophages after αCD40 injection, we analyzed the proliferation of macrophages by BrdU staining in the liver, bone marrow, and PBMCs. We injected 2 mg BrdU i.p. into mice at 2 h before sacrifice. Proliferation of $CD11b^+$ cells peaked in each tissue at Day 3 after injection and decreased by Day 5 (**Fig. 2A**), consistent with the numbers of the macrophage populations in the FACS analysis.

To determine whether differentiation from monocytes to tissue macrophages was induced in each tissue, we investigated the changes in the proportions of $Ly\text{-}6C^+$ and $F4/80^+$ cells among the $CD11b^+$ cells (Fig. 2B). $Ly\text{-}6C^-/F4/80^+/CD11b^+$ and $Ly\text{-}6C^+/F4/80^-/CD11b^+$ cells comprised the majority of cells in the liver after injection of the control antibody, and $Ly\text{-}6C^+/F4/80^+/CD11b^+$ cells increased at Day 1 and peaked at Day 3. These findings demonstrate that the proportion of $Ly\text{-}6C^-/F4/80^+/CD11b^+$ cells increased from Days 3 to 5, indicating that differentiation from monocytes to tissue macrophages had occurred by Day 3. In the bone marrow, $Ly\text{-}6C^+/F4/80^+/CD11b^+$ cells began to increase at Day 1 after αCD40 injection compared with the findings for the control antibody but had decreased by Day 5, indicating that αCD40 stimulation also induced the differentiation of macrophages. Similarly, $Ly\text{-}6C^+/F4/80^+/CD11b^+$ cells, among the PBMCs, began to increase by Day 1 after αCD40 injection and peaked at Day 3.

Role of NKT cells

To evaluate the role of NKT cells in this liver injury, NKT KO and C57BL/6 mice were injected with αCD40 and killed at Days 1 and 5. No significant difference between the serum ALT activities was observed after rat IgG injection, which is presented as Day 0, and NKT KO mice exhibited significantly lower serum ALT activities than WT mice at Days 1 and 5 ($P<0.05$; **Fig. 3A**). We also found that the absolute numbers of NK cells, T cells, macrophages, and neutrophils among the IHLs were reduced significantly in NKT KO mice (Fig. 3B). Consistent with the reduced number of IHLs in NKT KO mice, the IFN-γ, TNF-α, CCL2, and CCL5 mRNA expressions in the liver were suppressed at Days 1 and 5 after αCD40 injection (Fig. 3C and

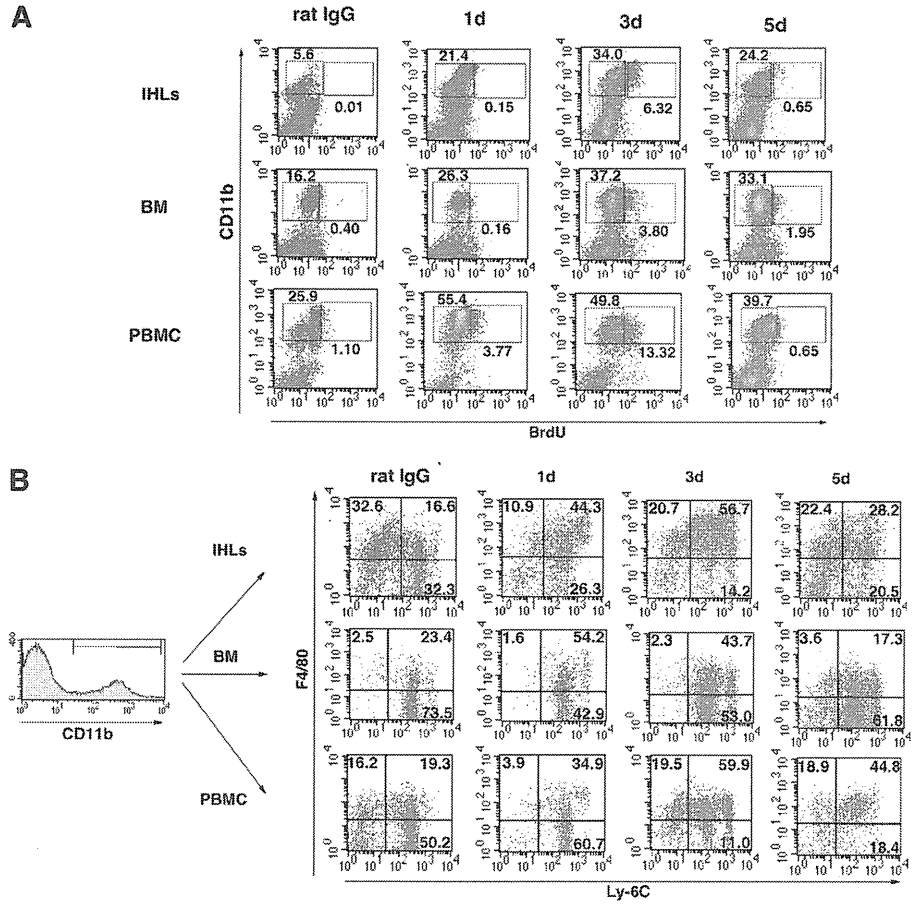

Figure 2. Macrophage differentiation and proliferation after αCD40 injection. (A) To analyze macrophage proliferation in IHLs, bone marrow (BM), and PBMCs after αCD40 injection, C57BL/6 mice were injected i.p. with 2 mg BrdU at 2 h before sacrifice. Cells were stained with anti-CD11b-allophycocyanin and anti-BrdU-FITC antibodies. (B) To analyze macrophage differentiation in IHLs, bone marrow, and PBMCs, cells were stained with anti-CD11b-allophycocyanin, anti-mouse F4/80-FITC, and anti-mouse Ly-6C-PE mAb.

D). We further found that the IFN-γ production by NK cells and TNF-α production by macrophages were suppressed in NKT KO mice (**Supplemental Fig. 3**). Furthermore, the serum IL-18 levels were reduced in NKT KO mice at Day 5 but not Day 1.

Finally, the numbers of Ly-6C^{++}/CD11b^{+}, Ly-6C^{+}/CD11b^{+}, and F4/80^{+}/CD11b^{+} cells in NKT KO mice were reduced significantly compared with WT mice at Day 5 after injection (Fig. 3E), demonstrating that NKT cells were involved in the macrophage and monocyte infiltration in the liver.

Depletion of neutrophils exacerbates the liver injury

To determine whether neutrophils play a role in this liver injury, we injected αCD40 into C57BL/6 mice with αGr-1 mAb or rat IgG2b at Days −1, +1, and +3. The mice were killed at Day 5. We confirmed that αGr-1 mAb treatment specifically depleted IHLs with an efficiency of >95% (Gr-1^{++}/CD11b^{+} cells), as evaluated by FACS analysis (Supplemental Fig. 4).

Administration of αGr-1 mAb significantly increased the serum ALT activity at Day 5 compared with the control antibody (P<0.05; **Fig. 4A**). Although the total number of IHLs decreased after αCD40 plus αGr-1 mAb treatment, the numbers of Gr-1^{+}/CD11b^{+} cells, including Ly-6C^{++}/CD11b^{+} and F4/80^{+}/CD11b^{+} cells, increased (Fig. 4B, C, and E). Immunohistochemical analyses revealed that Ly-6C^{+} and F4/80^{+} cells were increased in the liver at Day 5 after αCD40 mAb plus αGr-1 mAb treatment (Fig. 4F). Consistent with these observations, the serum TNF-α and IL-18 but not IFN-γ levels were elevated in the neutrophil-depleted state (Fig. 4D). In addition, TNF-α production by Ly-6C^{++}/CD11b^{+} and F4/80^{+}/CD11b^{+} cells was increased in αGr-1 mAb-treated mice (Fig. 4G), suggesting that neutrophils may play a suppressive role in macrophage recruitment and function in this liver inflammation.

Neutralization of IL-18 suppresses the liver injury

To assess whether IL-18 is responsible for the αCD40-induced liver injury, we injected C57BL/6 mice with αIL-18 mAb or rat IgG as a control at −1, +1, and 2 days after αCD40 injection and then killed the mice at Day 5. Administration of αIL-18 mAb significantly suppressed the serum ALT activity at Day 5 (P<0.05; **Fig. 5A**), demonstrating that IL-18 contributes to the liver injury. Consistent with this finding, αIL-18 mAb treatment decreased the IFN-γ and TNF-α mRNA expressions in the liver (Fig. 5B). We also found that αIL-18 mAb treatment inhibited the recruitment of macrophage subpopulations, neutrophils, NK cells, and T cells but not NKT cells into the liver (Fig. 5C). Immunohistochemical analyses revealed that Ly-6C^{+} and F4/80^{+} cells

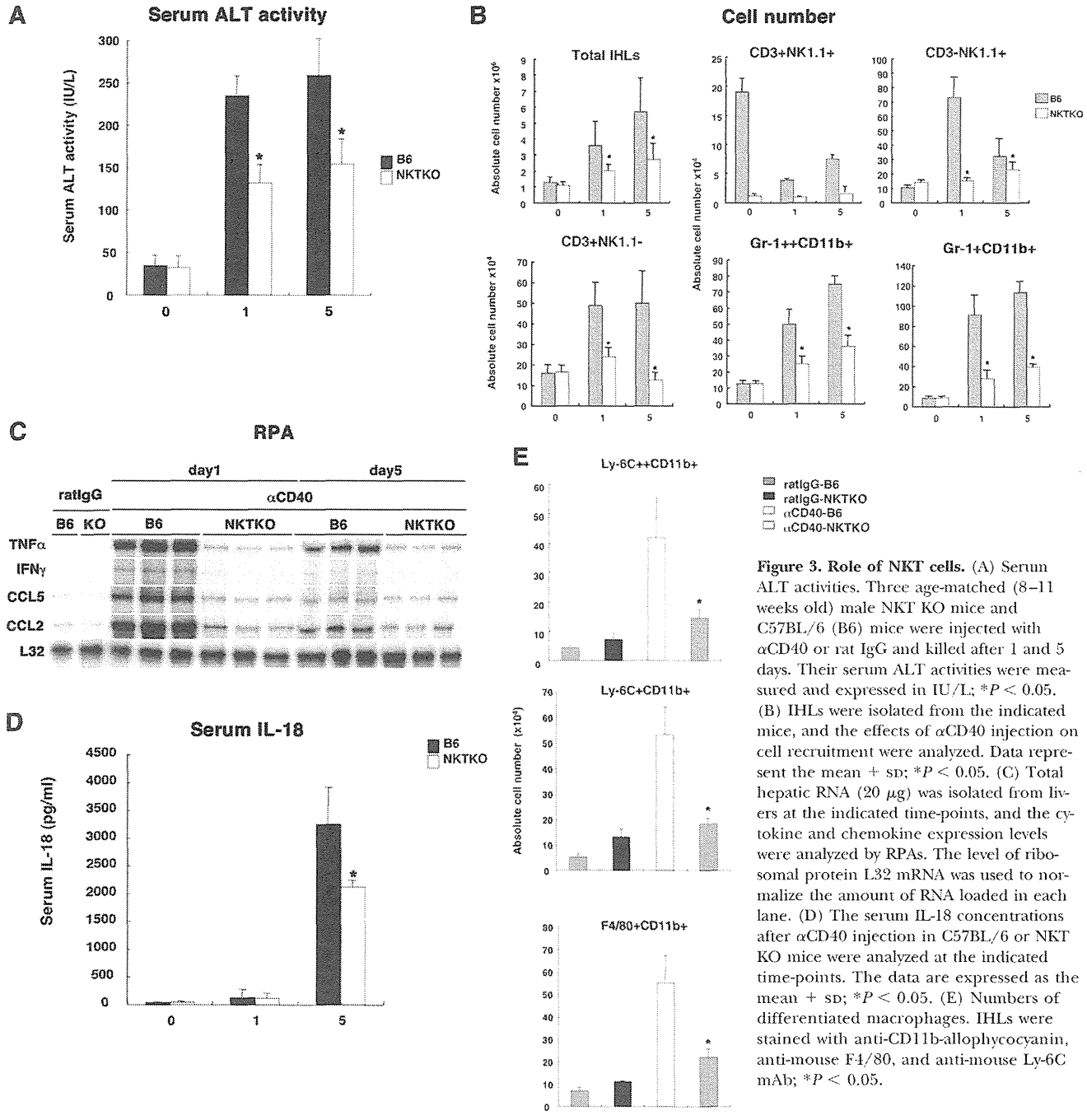

Figure 3. Role of NKT cells. (A) Serum ALT activities. Three age-matched (8–11 weeks old) male NKT KO mice and C57BL/6 (B6) mice were injected with αCD40 or rat IgG and killed after 1 and 5 days. Their serum ALT activities were measured and expressed in IU/L; $*P < 0.05$. (B) IHLs were isolated from the indicated mice, and the effects of αCD40 injection on cell recruitment were analyzed. Data represent the mean + SD; $*P < 0.05$. (C) Total hepatic RNA (20 μg) was isolated from livers at the indicated time-points, and the cytokine and chemokine expression levels were analyzed by RPAs. The level of ribosomal protein L32 mRNA was used to normalize the amount of RNA loaded in each lane. (D) The serum IL-18 concentrations after αCD40 injection in C57BL/6 or NKT KO mice were analyzed at the indicated time-points. The data are expressed as the mean + SD; $*P < 0.05$. (E) Numbers of differentiated macrophages. IHLs were stained with anti-CD11b-allophycocyanin, anti-mouse F4/80, and anti-mouse Ly-6C mAb; $*P < 0.05$.

were decreased in the liver at Day 5 after αCD40 mAb plus αIL-18 mAb treatment (Fig. 5D).

IL-18 causes severe liver injury with high levels of IFN-γ

To evaluate the effect of IL-18 on the late-phase liver injury, we i.p.-injected mice with 1 μg murine rIL-18 at 4 days after αCD40 injection and measured their serum ALT activity and inflammatory cytokine levels. The serum ALT activity was increased significantly by about four times after rIL-18 treatment compared with the control, although the number of IHLs, except for the macrophage population, was suppressed (**Fig. 6A–C**). In addition, serum IFN-γ was elevated significantly after injection of αCD40 with rIL-18, and NK cells strongly produced IFN-γ after rIL-18 treatment (Fig. 6D and E). In contrast, no difference was seen for TNF-α production by macrophages (Fig. 6E). Thus, IL-18 mainly activated NK cells and reduced the numbers of monocytes and neutrophils in the liver (Fig. 6A and B).

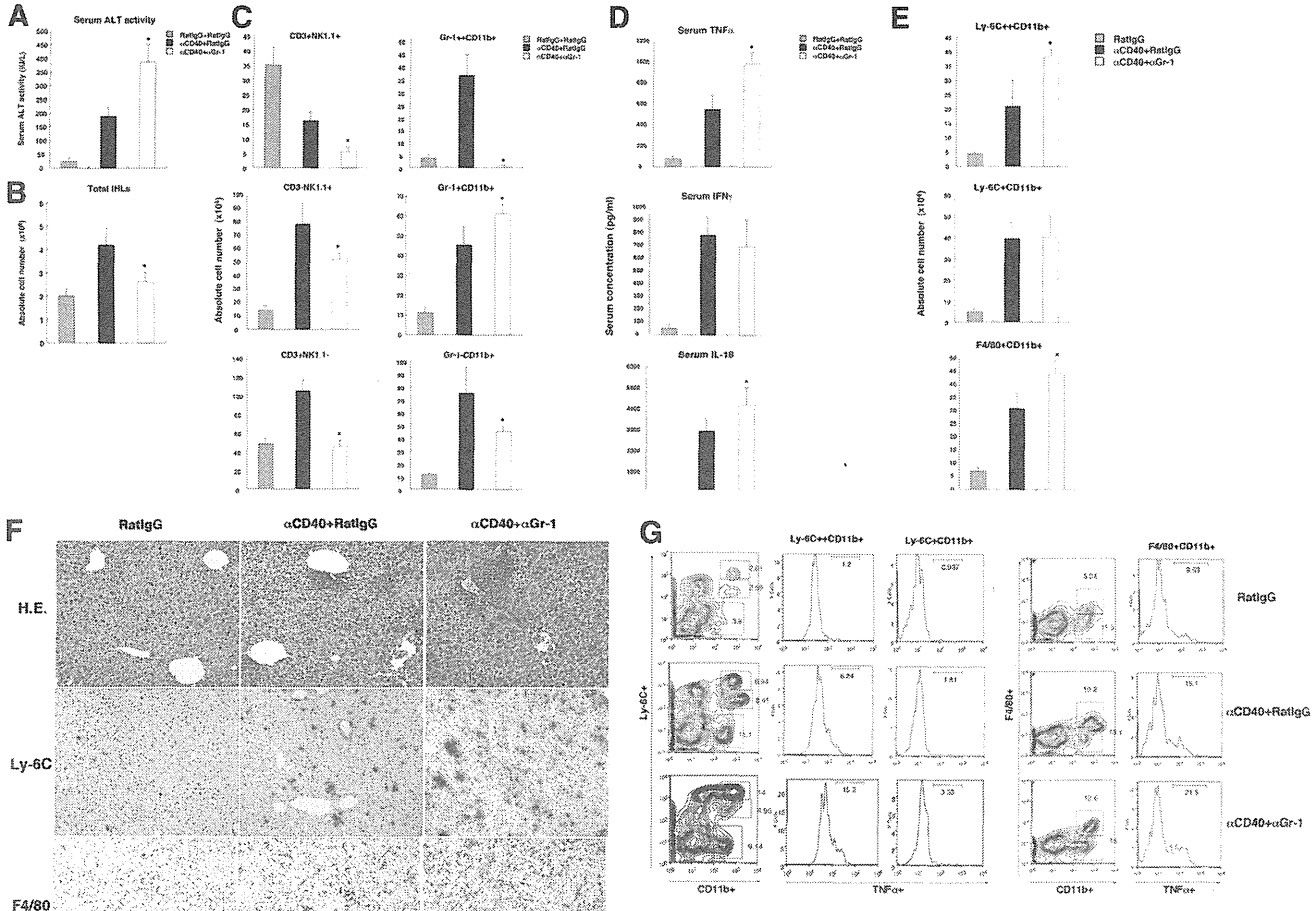

Figure 4. Role of neutrophils. (A) Serum ALT activities. C57BL/6 mice were injected with αCD40 or rat IgG in the absence or presence of αGr-1 mAb and killed after 5 days. Their serum ALT activities were measured and expressed in IU/L; $^*P < 0.05$. (B and C) IHLs were isolated from the indicated mice, and the effects of αGr-1 mAb on cell recruitment were analyzed. Data represent the mean + SD; $^*P < 0.05$. (D) Serum cytokine concentrations after αCD40 injection in C57BL/6 mice. Data are expressed as the mean + SD; $^*P < 0.05$. (E) Numbers of differentiated macrophages. IHLs were stained with anti-CD11b-allophycocyanin, anti-mouse F4/80, and anti-mouse Ly-6C mAb; $^*P < 0.05$. (F) Immunohistochemical staining. Liver sections obtained from mice killed at 5 days after injection were stained with H&E or with anti-mouse F4/80, Ly-6C, or Gr-1 mAb. (G) Intracellular cytokine expression levels in macrophages and monocytes. To determine which cell populations produced TNF-α after injection, we stained the cells with anti-mouse F4/80-FITC, Ly-6C-PE, anti-CD11b-allophycocyanin, and anti-TNF-α-PE mAb. The cells were analyzed using a FACSCalibur system.

DISCUSSION

The present study has clarified several important aspects of liver pathology in terms of inflammatory cell recruitment and activation in the liver and provides important findings regarding the interactions among IL-18, macrophages, neutrophils, and NKT cells. The innate immune system, which is considered to provide nonantigen-specific immune responses, can provide emergency signals from destroyed hepatocytes during liver inflammation, resulting in an inflammatory response. These inflammatory events contribute to liver injury and conversely, may also be involved in liver repair based on various experimental liver disease models [18–20]. Therefore, it is well established that an inflammatory response is essential for controlling the microenvironment in the liver, but the relationships among macrophages and other inflammatory cells with regard to liver injury are still obscure. Careful interpretation is required to evaluate the results of the present study, especially with regard to the interactions between IHLs and the liver injury in this model. The liver injury model that we used involves artificial stimulation of macrophages, monocytes, and B cells that express CD40, and these cells subsequently activate NK cells and NKT cells, thereby causing liver injury by way of IFN-γ, TNF-α, and IL-12 [14, 15]. In general, it has

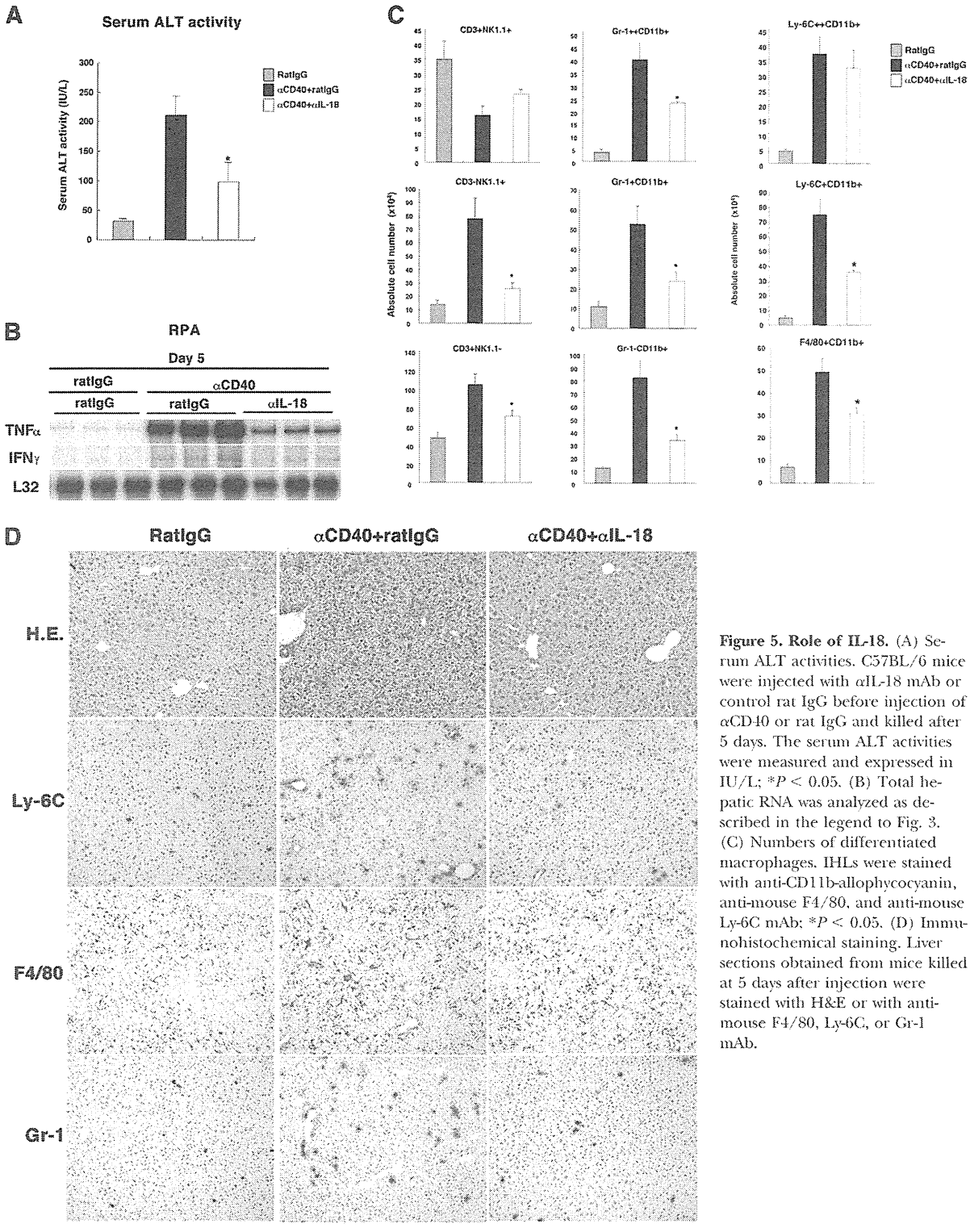

Figure 5. Role of IL-18. (A) Serum ALT activities. C57BL/6 mice were injected with αIL-18 mAb or control rat IgG before injection of αCD40 or rat IgG and killed after 5 days. The serum ALT activities were measured and expressed in IU/L; $^*P < 0.05$. (B) Total hepatic RNA was analyzed as described in the legend to Fig. 3. (C) Numbers of differentiated macrophages. IHLs were stained with anti-CD11b-allophycocyanin, anti-mouse F4/80, and anti-mouse Ly-6C mAb; $^*P < 0.05$. (D) Immunohistochemical staining. Liver sections obtained from mice killed at 5 days after injection were stained with H&E or with anti-mouse F4/80, Ly-6C, or Gr-1 mAb.

been well understood that the interactions between CD40 and CD40 ligand reciprocally deliver activating signals to APCs and cognate T cells. This process is critically important for the development of adaptive immunity [21–23]. However, we consider that this liver injury model is useful for analyzing how activated macrophages or B cells affect the activation of other IHLs and their recruitment in liver injury, as the agonistic CD40 antibody mainly activates macrophages and B cells.

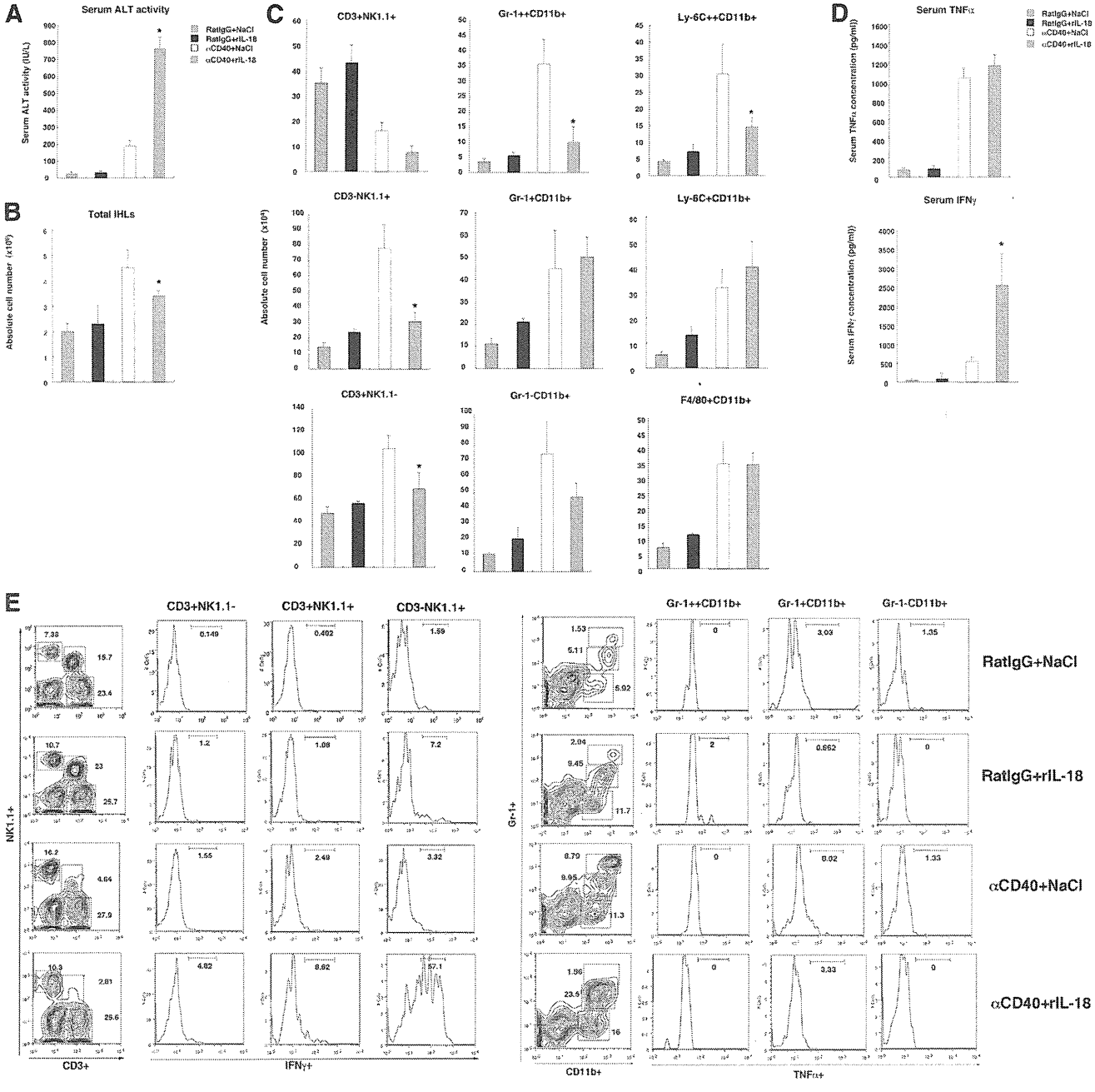

Figure 6. Additional IL-18 treatment exacerbates liver injury after αCD40 injection. (A) Serum ALT activities. C57BL/6 mice were injected with αCD40 or rat IgG in the absence or presence of rIL-18 and killed after 5 days. The serum ALT activities were measured and expressed in IU/L; $^*P < 0.05$. (B and C) IHLs were isolated from the indicated mice, and the effects of IL-18 on cell recruitment were analyzed. Data represent the mean + SD; $^*P < 0.05$. (D) Serum cytokine concentrations after αCD40 injection in C57BL/6 mice. Data are expressed as the mean + SD; $^*P < 0.05$. (E) Intracellular cytokine expression levels in macrophages and monocytes. To determine which cell populations produced TNF-α after injection, we stained the cells with anti-mouse F4/80-FITC, Ly-6C-PE, anti-CD11b-allophycocyanin, and anti-TNF-α-PE mAb. The cells were analyzed using a FACSCalibur system.

First, we determined the characteristics of intrahepatic macrophages, which became activated on Days 1 and 5 after αCD40 injection, as they are key effector cells for the liver injury [14]. We analyzed the proliferation of the macrophages and detected a peak at Day 3. This finding was consistent with the observed numbers of macrophages. Notably, the highly proliferating macrophages were unable to produce TNF-α, and this is considered to be one of the reasons why αCD40-triggered inflammation exhibits a biphasic pattern in the liver. The present study demonstrated that monocyte subsets differing in Ly-6C expression represented different stages in

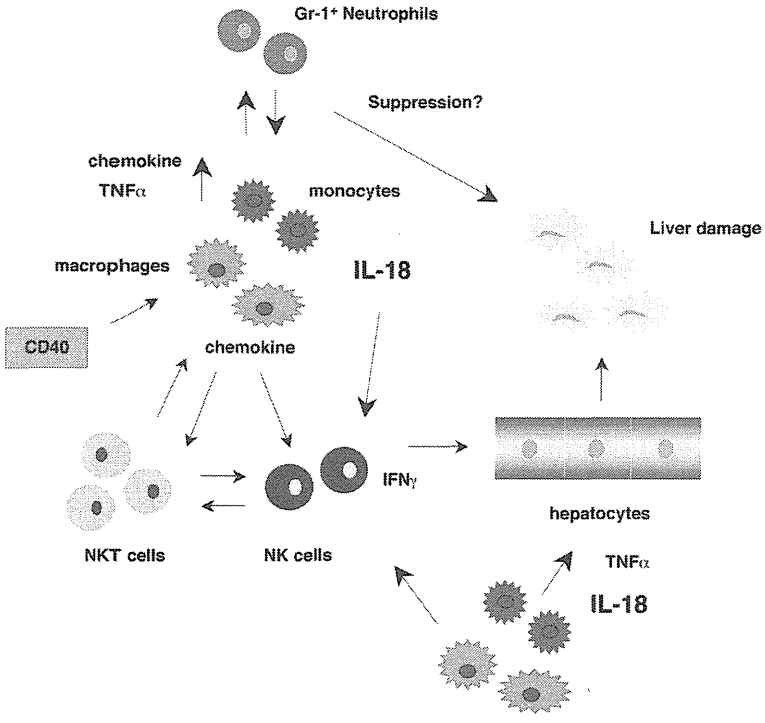

Figure 7. Scheme for how αCD40 triggers liver inflammation. 1) TNF-α and chemokines are produced by activated macrophages after αCD40 stimulation. 2) Neutrophils increase rapidly and control the activation of macrophages or monocytes. 3) At the same time, NKT cells are activated and produce inflammatory cytokines. 4) IL-18 stimulates the migration of macrophages and monocytes into the liver and activates NK cells. 5) Inflammatory cytokines stimulate IFN-γ production by NK cells, and the produced IFN-γ further stimulates macrophages and exacerbates the severe liver injury.

a continuous maturation pathway, and previous in vitro experiments indicated that this transition occurs within 24–48 h [24]. Based on these findings, we suggest that not only the increase in Ly-6C^{high} monocytes, which have suppressive functions [25], but also the high proliferation of macrophages may cause the suppressed inflammatory response at Day 3. Although we investigated the suppressive inflammatory cytokine IL-10, we were unable to confirm the elevated production of this cytokine in the liver at Day 3 compared with Day 5 (Supplemental Fig. 1).

Although tissue macrophages and monocytes increased to reach a peak at Day 3 after injection, neutrophils increased rapidly and were reduced by Day 3. Interestingly, we found that neutrophil depletion exacerbated the αCD40-induced liver injury. In general, neutrophils have an effector function against several liver injury models, such as those involving carbon tetrachloride- and ischemic/perfusion-induced liver injury [26, 27]. These previous studies demonstrated that reactive oxygen from neutrophils is a key factor for hepatocyte damage. Our findings seem to be contradictory to the well-established paradigm that neutrophils induce tissue damage. However, the outcomes of αGr-1 treatment may vary depending on the liver injury models involved, as we have shown already that αGr-1 treatment partially protects against liver injury in hepatitis B virus transgenic mice [28, 29].

A recent report suggested that Gr-1^{high}CD11b^{+} cells suppress T cells in tumor-bearing mice [30] and that Gr-1^{high}CD11b^{low} polymononuclear cell–myeloid-derived suppressor cell populations have suppressive potential in the healthy spleen [31]. These reports suggest the possibility that liver injury is exacerbated by depletion of suppressive, Gr-1-positive cells. Furthermore, we need to confirm whether antibody-tagged neutrophils accumulate in the liver and whether Kupffer cells are activated by phagocytosis. In fact, we found that αGr-1 treatment induced the migration of macrophages and monocytes into the liver, and these cells produced large amounts of TNF-α, indicating that conclusive evidence for whether neutrophils have suppressive effects on this liver injury may require further investigations.

We further found that NKT cells participated in the αCD40-induced biphasic liver injury. NKT cells are particularly abundant in the liver, accounting for 20–30% of IHLs, and are thought to play roles in immunity against intracellular bacteria and parasites and certain tumors [8, 32]. It is well established that CD40 cross-linking induces DCs to up-regulate their expressions of CD40, B7.1, B7.2, and IL-12, which in turn, enhance NKT cell activation and cytokine production [32]. In this liver injury, NKT cells activated other inflammatory cells, including NK cells and macrophages, in the liver, as IFN-γ production by NK cells and TNF-α production by macrophages were apparently blocked in the liver of NKT KO mice. Consistent with the finding that macrophage recruitment was reduced in NKT KO mice, infiltration of the various macrophage subpopulations was also inhibited, indicating that NKT cells have an influence on macrophage differentiation following αCD40 injection. It is of note that NKT cells were secondarily activated by way of CD40 ligation on macrophages and DCs and that NKT KO mice appear to exhibit protection against inflammatory cell recruitment into the liver. These findings demonstrate the importance of NKT cells for the propagation of inflammatory liver disease.

In this study, we have demonstrated that IL-18 is involved in the late-phase liver injury. Although we found that IL-12 played a pivotal role in the early-phase liver injury, IL-18 was not necessary for liver injury to occur, as neutralization of IL-18 did not increase the serum ALT activity (Supplemental Fig. 5). IL-18 is known to induce NK and NKT cells to produce IFN-γ [12], but it

requires IL-12 to induce IFN-γ production by Th1 cells [11]. In keeping with these findings, we found that rIL-18 treatment rapidly induced intrahepatic NK cells to produce large amounts of IFN-γ and also to cause severe liver injury. Importantly, these effects did not involve TNF-α and did not require the recruitment of macrophages, monocytes, and neutrophils into the liver. More recently, intracellular microbial sensors have been identified, including NLRs [33, 34]. Some of the NLRs also sense nonmicrobial danger signals and form large cytoplasmic complexes called inflammasomes, which link the sensing of microbial products and metabolic stress to proteolytic activation of the proinflammatory cytokines IL-1β and IL-18. Therefore, in this model, the danger signals for early liver damage may trigger the activation of inflammasomes, resulting in the production of IL-18 and subsequent induction of liver damage.

In conclusion, the present results demonstrate that activation of intrahepatic macrophages can initiate a cascade of events that begins with the production of inflammatory cytokines and chemokines and leads to the activation of intrahepatic NK and NKT cells for the production of IFN-γ, all of which contribute to the recruitment of additional inflammatory cells to the liver (**Fig. 7**). We have shown that the interactions among macrophages, monocytes, neutrophils, and NKT cells participate efficiently and closely in the exacerbation of liver inflammation through cytokine and chemokine production. Further studies are required to identify the roles of the suppressive monocyte or neutrophil subpopulations in the liver injury, and clarification of the roles of these cell types will be useful in the treatment of various liver diseases.

AUTHORSHIP

K.K. planned the experimental project, and K.K., S.S., S.H., Y.H., T.H., and M.N. performed data analysis and wrote the paper. M.K. contributed data and comments about the manuscript.

ACKNOWLEDGMENTS

This study was supported by a grant-in-aid (B) from the Ministry of Education, Culture, Sports, Science and Technology of Japan (grant no. 20390203) and a grant-in-aid for specially promoted research on viral diseases from the Tokyo Metropolitan Government to K.K. We thank Dr. Francis V. Chisari (The Scripps Research Institute) for supporting this study and Dr. Antonius Rolink (Basel Institute for Immunology) for providing the anti-mouse agonistic CD40 mAb. We are also grateful to Drs. Toshinori Nakayama (Chiba University) and Masaru Taniguchi (RIKEN) for providing the Vα14 NKT KO mice.

REFERENCES

1. Akira, S., Uematsu, S., Takeuchi, O. (2006) Pathogen recognition and innate immunity. *Cell* **124,** 783–801.
2. Crispe, I. N. (2009) The liver as a lymphoid organ. *Annu. Rev. Immunol.* **27,** 147–163.
3. Crispe, I. N. (2003) Hepatic T cells and liver tolerance. *Nat. Rev. Immunol.* **3,** 51–62.
4. Banchereau, J., Briere, F., Caux, C., Davoust, J., Lebecque, S., Liu, Y. J., Pulendran, B., Palucka, K. (2000) Immunobiology of dendritic cells. *Annu. Rev. Immunol.* **18,** 767–811.
5. Munder, M., Mallo, M., Eichmann, K., Modolell, M. (1998) Murine macrophages secrete interferon γ upon combined stimulation with interleukin (IL)-12 and IL-18: a novel pathway of autocrine macrophage activation. *J. Exp. Med.* **187,** 2103–2108.
6. Zlotnik, A., Yoshie, O. (2000) Chemokines: a new classification system and their role in immunity. *Immunity* **12,** 121–127.
7. Wardle, E. N. (1987) Kupffer cells and their function. *Liver* **7,** 63–75.
8. Taniguchi, M., Harada, M., Kojo, S., Nakayama, T., Wakao, H. (2003) The regulatory role of Vα14 NKT cells in innate and acquired immune response. *Annu. Rev. Immunol.* **21,** 483–513.
9. Seino, K., Taniguchi, M. (2005) Functionally distinct NKT cell subsets and subtypes. *J. Exp. Med.* **202,** 1623–1626.
10. Van Kaer, L., Joyce, S. (2005) Innate immunity: NKT cells in the spotlight. *Curr. Biol.* **15,** R429–R431.
11. Nakanishi, K., Yoshimoto, T., Tsutsui, H., Okamura, H. (2001) Interleukin-18 regulates both Th1 and Th2 responses. *Annu. Rev. Immunol.* **19,** 423–474.
12. Okamura, H., Kashiwamura, S., Tsutsui, H., Yoshimoto, T., Nakanishi, K. (1998) Regulation of interferon-γ production by IL-12 and IL-18. *Curr. Opin. Immunol.* **10,** 259–264.
13. Kimura, K., Kakimi, K., Wieland, S., Guidotti, L. G., Chisari, F. V. (2002) Interleukin-18 inhibits hepatitis B virus replication in the livers of transgenic mice. *J. Virol.* **76,** 10702–10707.
14. Kimura, K., Kakimi, K., Wieland, S., Guidotti, L. G., Chisari, F. V. (2002) Activated intrahepatic antigen-presenting cells inhibit hepatitis B virus replication in the liver of transgenic mice. *J. Immunol.* **169,** 5188–5195.
15. Kimura, K., Moriwaki, H., Nagaki, M., Saio, M., Nakamoto, Y., Naito, M., Kuwata, K., Chisari, F. V. (2006) Pathogenic role of B cells in anti-CD40-induced necroinflammatory liver disease. *Am. J. Pathol.* **168,** 786–795.
16. Rolink, A., Melchers, F., Andersson, J. (1996) The SCID but not the RAG-2 gene product is required for S μ-S ε heavy chain class switching. *Immunity* **5,** 319–330.
17. Naito, M., Nagai, H., Kawano, S., Umezu, H., Zhu, H., Moriyama, H., Yamamoto, T., Takatsuka, H., Takei, Y. (1996) Liposome-encapsulated dichloromethylene diphosphonate induces macrophage apoptosis in vivo and in vitro. *J. Leukoc. Biol.* **60,** 337–344.
18. Gao, B., Jeong, W. I., Tian, Z. (2008) Liver: an organ with predominant innate immunity. *Hepatology* **47,** 729–736.
19. Guidotti, L. G., Chisari, F. V. (2001) Noncytolytic control of viral infections by the innate and adaptive immune response. *Annu. Rev. Immunol.* **19,** 65–91.
20. Jaeschke, H., Bajt, M. L. (2004) Critical role of CXC chemokines in endotoxemic liver injury in mice. *J. Leukoc. Biol.* **76,** 1089–1090, author reply 1091–1092.
21. Banchereau, J., Bazan, F., Blanchard, D., Briere, F., Galizzi, J. P., van Kooten, C., Liu, Y. J., Rousset, F., Saeland, S. (1994) The CD40 antigen and its ligand. *Annu. Rev. Immunol.* **12,** 881–922.
22. Cella, M., Scheidegger, D., Palmer-Lehmann, K., Lane, P., Lanzavecchia, A., Alber, G. (1996) Ligation of CD40 on dendritic cells triggers production of high levels of interleukin-12 and enhances T cell stimulatory capacity: T-T help via APC activation. *J. Exp. Med.* **184,** 747–752.
23. Grewal, I. S., Flavell, R. A. (1998) CD40 and CD154 in cell-mediated immunity. *Annu. Rev. Immunol.* **16,** 111–135.
24. Leenen, P. J., de Bruijn, M. F., Voerman, J. S., Campbell, P. A., van Ewijk, W. (1994) Markers of mouse macrophage development detected by monoclonal antibodies. *J. Immunol. Methods* **174,** 5–19.
25. Zhu, B., Bando, Y., Xiao, S., Yang, K., Anderson, A. C., Kuchroo, V. K., Khoury, S. J. (2007) CD11b+Ly-6C(hi) suppressive monocytes in experimental autoimmune encephalomyelitis. *J. Immunol.* **179,** 5228–5237.
26. Duffield, J. S., Forbes, S. J., Constandinou, C. M., Clay, S., Partolina, M., Vuthoori, S., Wu, S., Lang, R., Iredale, J. P. (2005) Selective depletion of macrophages reveals distinct, opposing roles during liver injury and repair. *J. Clin. Invest.* **115,** 56–65.
27. Luster, M. I., Simeonova, P. P., Gallucci, R. M., Bruccoleri, A., Blazka, M. E., Yucesoy, B. (2001) Role of inflammation in chemical-induced hepatotoxicity. *Toxicol. Lett.* **120,** 317–321.
28. Takai, S., Kimura, K., Nagaki, M., Satake, S., Kakimi, K., Moriwaki, H. (2005) Blockade of neutrophil elastase attenuates severe liver injury in hepatitis B transgenic mice. *J. Virol.* **79,** 15142–15150.
29. Sitia, G., Isogawa, M., Kakimi, K., Wieland, S. F., Chisari, F. V., Guidotti, L. G. (2002) Depletion of neutrophils blocks the recruitment of antigen-nonspecific cells into the liver without affecting the antiviral activity of hepatitis B virus-specific cytotoxic T lymphocytes. *Proc. Natl. Acad. Sci. USA* **99,** 13717–13722.
30. Dolcetti, L., Peranzoni, E., Ugel, S., Marigo, I., Fernandez Gomez, A., Mesa, C., Geilich, M., Winkels, G., Traggiai, E., Casati, A., Grassi, F., Bronte, V. (2010) Hierarchy of immunosuppressive strength among myeloid-derived suppressor cell subsets is determined by GM-CSF. *Eur. J. Immunol.* **40,** 22–35.
31. Greifenberg, V., Ribechini, E., Rossner, S., Lutz, M. B. (2009) Myeloid-derived suppressor cell activation by combined LPS and IFN-γ treatment impairs DC development. *Eur. J. Immunol.* **39,** 2865–2876.
32. Kronenberg, M. (2005) Toward an understanding of NKT cell biology: progress and paradoxes. *Annu. Rev. Immunol.* **23,** 877–900.
33. Martinon, F., Mayor, A., Tschopp, J. (2009) The inflammasomes: guardians of the body. *Annu. Rev. Immunol.* **27,** 229–265.
34. Pétrilli, V., Dostert, C., Muruve, D. A., Tschopp, J. (2007) The inflammasome: a danger sensing complex triggering innate immunity. *Curr. Opin. Immunol.* **19,** 615–622.

KEY WORDS:
neutrophil · macrophage · NKT cell · chemokine · IL-18

Exp. Anim. 60(2), 93–100, 2011

—Review—
Review Series: Frontiers of Model Animals for Human Diseases

An Experimental Mouse Model for Hepatitis C Virus

Kiminori KIMURA[1,2] and Michinori KOHARA[1]

[1]*Department of Microbiology and Cell Biology, Tokyo Metropolitan Institute of Medical Science, Tokyo 156-8506 and* [2]*Division of Hepatology, Tokyo Metropolitan Cancer and Infectious Diseases Center, Komagome Hospital, Tokyo 113-8677, Japan*

Abstract: Chronic hepatitis C virus (HCV) infection affects approximately 170 million people and is a major global health problem because infected individuals can develop liver cirrhosis and hepatocellular carcinoma. Despite significant improvements in antiviral drugs, only around 50% of treated patients with genotype 1 and 4 demonstrate HCV clearance. Unfortunately, an anti-HCV vaccine is still not available. To progress treatment of HCV, it is necessary to understand the mechanism(s) by which HCV infects hepatocytes, and how the host immune response prevents the spread of the virus. Because HCV infects only humans and chimpanzees, it is difficult to evaluate immune response mechanisms, and the effects of chemicals and new technologies on these response mechanisms. These difficulties underline the importance of establishing a small HCV-infected animal model. This review focuses on the progress made in recent years towards the development of an experimental mouse model for HCV.

Key words: apoptosis, B cell lymphoma, HCV, immune response, transgenic mice

Introduction

Hepatitis C virus (HCV) is a non-cytopathic, hepatotropic member of the *Flaviviridae* family, causing acute and chronic necroinflammatory liver diseases [25]. Chronic HCV infection has caused an epidemic with approximately 170 million people infected worldwide and three to four million people newly infected each year [25, 35]. Natural history studies show that 5–20% of patients develop cirrhosis after about 20 years of infection [1, 42, 49]. An increasing number of patients with cirrhosis will develop hepatocellular carcinoma. End-stage liver disease due to chronic HCV infection is the leading cause of liver transplantation in the western world [36]. Furthermore, co-infection with HCV and human immunodeficiency virus (HIV) results in more serious liver cirrhosis than HCV infection alone and the mortality of HIV-infected HCV patients is a serious problem in the USA [44, 55].

The HCV genome is a 9.6-kb, uncapped, linear, single-strand RNA molecule with positive polarity that serves as a template for both translation and replication. Translation of the plus-strand RNA initiates at an internal ribosomal entry site, resulting in the production of a single polyprotein precursor that is processed into structural (C, E1, E2, p7) and non-structural (NS2, NS3, NS4A, NS4B, NS5A, and NS5B) protein subunits by host and viral proteases [8, 9, 37, 46]. Because of the lack of a proofreading func-

(Received 20 December 2010 / Accepted 29 January 2010)

Address corresponding: M. Kohara, Department of Microbiology and Cell Biology, Tokyo Metropolitan Institute of Medical Science, 2–1–6 Kamikitazawa, Setagaya-ku, Tokyo 156-8506, Japan